2-1-2008

Design and optimization of input shapers for liquid slosh suppression

Ameen Aboel Hassan

THE AMERICAN UNIVERSITY IN CAIRO

SCHOOL OF SCIENCES AND ENGINEERING

Design and Optimization of Input Shapers for Liquid Slosh Suppression

By

Ameen Roshdy Aboel Hassan

A thesis submitted in partial fulfillment of the requirements for the degree of

Master of Science in Engineering

With specialization in:

Design

Under supervision of:

Dr. Mustafa Arafa
Assistant Professor, Mechanical Engineering Department
and
Dr. Ashraf Nassef
Associate Professor, Mechanical Engineering Department

SUMMER 2007

ACKNOWLEDGEMENT

I would like to thank my father who will always be my reference in life, who instilled in me the seriousness, the rectitude, and most importantly love of life and faith in justice. To my mother I offer my sincere affection, her place in my heart will never be replaced. My memories with my family will remain the guiding lighthouse for my life.

I would like to thank Dr. Mustafa Arafa who was most understanding and tolerant. Without his guidance and constant support, this work could have never been done. I would like also, to thank Dr. Ashraf Nassef for his support and encouragement both inside and outside academic scope.

I'm indebted to huge number of people who helped me in an outstanding way all through my life. I hope I live up to their expectations and be able to show gratitude by helping others when I get the chance.

ABSTRACT

The need for fast maneuvering and accurate positioning of flexible structures poses a control challenge. The flexibility inherent in these lightly damped systems creates large residual vibrations in response to fast disturbances. Several control approaches have been proposed to tackle this class of problems, of which the input shaping technique seems quite appealing.

While input shaping has been widely investigated to attenuate residual vibrations in flexible structures, less attention was granted to expand its viability in further applications. It is therefore the aim of this work to develop a methodology for applying input shaping techniques to suppress sloshing effects in open moving containers to facilitate safe and fast point-to-point movements. The liquid behavior is modeled using finite element analysis. The input shaper parameters are optimized to find the commands that would result in minimum residual vibration. Other objectives, such as improved robustness and motion constraints such as deflection limiting are also included in the optimization scheme. Numerical results are verified on an experimental setup consisting of a small motor-driven water tank that is precisely guided to undergo rectilinear motion, while measuring both the tank motion and free surface displacement of the water. The results obtained suggest that input shaping is an effective method for suppressing residual liquid vibrations.

TABLE OF CONTENT

LIST OF FIGURES

LIST OF TABLES

NOMENCLATURE

Θ : Angular deflection of the payload of a gantry crane model.

x : Cart/Trolley position along the x direction.

$\dot{x}$: Cart/Trolley velocity along the x direction.

ω_n : System's natural frequency.

ζ : System's viscous damping ratio.

A_i : Amplitude of the i^{th} impulse (absolute value).

t_i : Time location of the i^{th} impulse.

$\Theta(t)_{total}$: Resultant angular deflection of the pay load of a gantry crane.

ω_d : Damped natural frequency.

$\theta_{\%\ residual}$: Percentage residual vibration of a unity impulse applied at t = 0.

ZV: Zero-Vibration input shaper.

ZVD: Zero-Vibration-Derivative input shaper.

DL: Deflection limiting input shaper.

EI: Extra-Insensitive input shaper.

K: Gain value of the proportional controller of the position closed-loop.

X_{ref}: Desired final position value.

$X_{shaped:}$ Commanded position based on the shaper parameters.

I_m: Motor current.

K_m: Motor back emf constant.

K_g: Motor gear box ratio.

r: Motor pinion radius

R : Cart position encoder radius.

V: voltage applied to the motor.

C_1: Term combining voltage constants of the DC motor ($C_1 = \frac{K_m K_g}{R \times r}$)

C_2: Term combining back emf constants of the DC motor ($C_2 = \frac{K_m^2 K_g^2}{R \times r^2}$)

M_{cart} : Cart Mass

N : Normal reaction at the linear bearing in the cart.

$sign$: Sign function (1 for all values ≥ 0, -1 for all values ≤ 0)

μ_k : Dynamic friction coefficient at the cart linear bearing

h : water height in the partially filled tank.

m_n: The value of the mass representing the n^{th} mode in the mechanical model

k_n: the value of the stiffness representing the n^{th} mode in the mechanical model

m_{liq}: Total mass of the liquid in the container

FE: Finite element model.

ρ : Fluid density.

w_I : Position of the left-side wall of the tank.

w_{II} : Position of the bottom of the tank.

w_{III} : Position of the right-side wall of the tank.

f_I : Force applied at the left-side wall of the tank.

f_{II} : Force applied at the bottom of the tank.

f_{III} : Force applied at the right-side of the tank.

k : stiffness of the rigid piston element.

$[M_{ff}]$, $\{M_{12\to 14}\}$, $m_{22\to 44}$: Elements in the FE mass matrix.

$[K_{11}]$, $\{K_{21\to 41}\}$: Elements in the FE stiffness matrix.

p_f : Pressure of the free water surface.

$x_1 \Rightarrow x_{n+4 \rightarrow 2n+4}$: Numerical model states.

$f_{friction}$: Friction force applied at the linear bearing.

U_i : Displacement of the ith node of the FE model.

c_i : factor vector in the objective function = [1,0.75,0.5]

$k_{1 \rightarrow 4}$: weighting factor in the objective function.

$H_{nominal}$: Water height at which the input shaper is designed.

CHAPTER 1

INTRODUCTION AND LITERATURE REVIEW

This chapter gives an overview of the input shaping technique, and provides a brief mathematical derivation of the simplest forms of input shapers. Next, the motivation, objectives and approach of this research work are discussed. A summary of the trends in input shaping research is presented, followed by the scientific contribution of the work performed in this thesis. The last section is an outline of the following chapters.

1.1. OVERVIEW OF INPUT SHAPING METHOD

The need for fast maneuvering and accurate positioning of flexible structures, poses a great control challenge. The flexibility inherent in these lightly damped systems creates large residual vibrations in response to fast disturbances resulting in either inaccurate positioning or time waste waiting for the residual vibration to die out. In some applications, safety issues may limit the amount of tolerable vibrations. For example, in ship yards or steel mills, swaying gantry cranes may result in serious safety hazards. In satellite movement, the stresses created due to antennas' vibration may result in failure or damage of the antenna [1]. Such problems were mitigated traditionally either by slowing down the movement, or by introducing more damping and mass in the structure. Therefore, most cranes for example have to be driven in a slower rate than the capability of their motors only to limit the sway of the payload. Needless to say, adding physical damping or mass is again a waste of time and energy.

There are numerous control techniques in the literature addressing the control of flexible structures to produce fast and accurate maneuvering while dampening their undesirable dynamics. These techniques can be grouped into three main categories, time-optimal, feedback, and command shaping. Time-optimal is the least adopted scheme in commercial use, since it requires a pre-computation of the entire command, thus preventing real-time control [2]. Feedback and command shaping are both implemented in various commercial applications.

Command shaping has received special attention since the seminal work of Singer and Seering [1]. The power of command shaping – also referred to as input shaping – is that it is a feedforward scheme, which does not require sensor feedback. Therefore, input shaping is usually cheap and easy to implement. However, as a feedforward approach, it suffers from sensitivity to modeling error and consequently becomes limited to a rather narrow range of parameters variation.

The basic idea behind input shaping is exciting the flexible modes of the system in such a way that they would combine destructively resulting in a low level of vibration at the end of the command. For example, in the case of gantry cranes the structure can be modeled, without loss of generality, as a cart-pendulum system, where the pendulum represents the pay load while the cart represents the trolley movement. Fig. 1-1 shows the pay load response for an impulse command. The first impulse initiated the response shown in blue. If the second impulse is adjusted with the correct time delay and amplitude to produce the exact negative of the first impulse as shown in green, the resultant vibration after the second impulse will reduce to zero as shown Fig. 1-2.

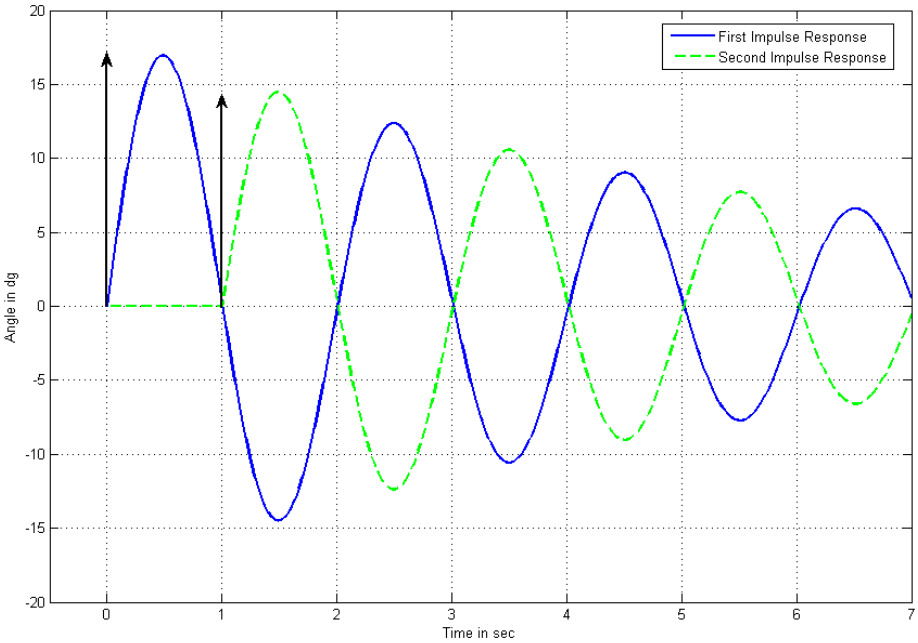

Figure 1-1 Impulse Response of Second Order System

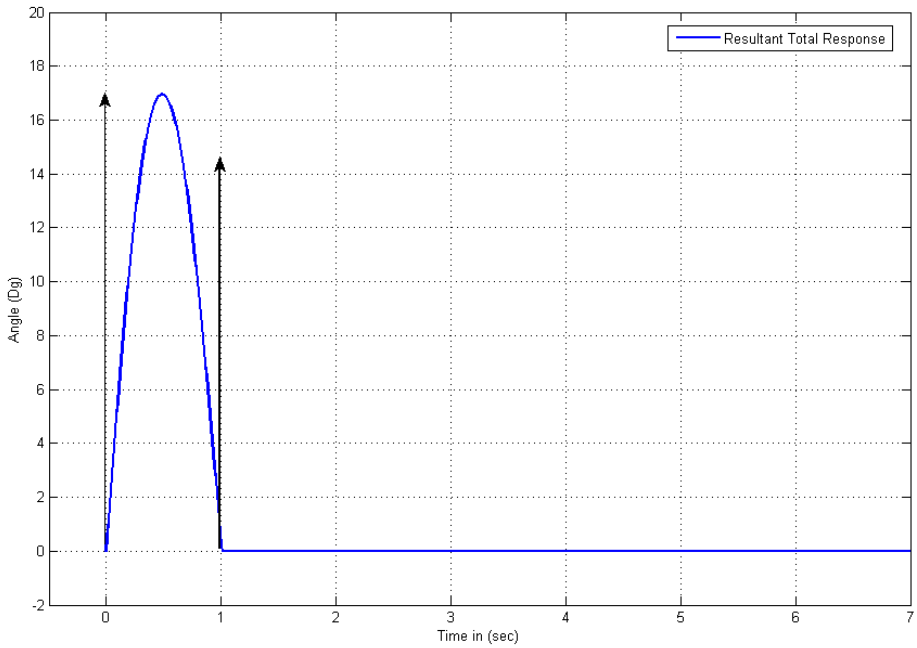

Figure 1-2 Resultant Response of two shaped impulses

This method can be applied in real time by convolving the set of the shaped impulses with the reference command to produce a shaped input command that results in a zero vibration, as shown in Fig. 1-3.

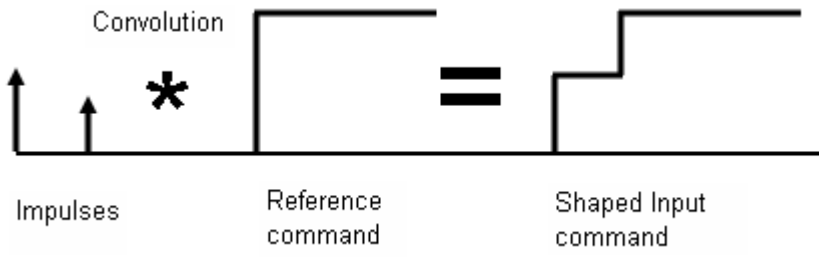

Figure 1-3 Input Shaper Filtering

Figure 1-4 shows a comparison between a step input and shaped input of trolley velocity in a lightly damped trolley-pendulum second order system. The blue curve is the response due to step input, while the red curve is the response of the shaped input (shown in green). The fast settling time of the shaped input comes at the cost of a small increase in the rise time.

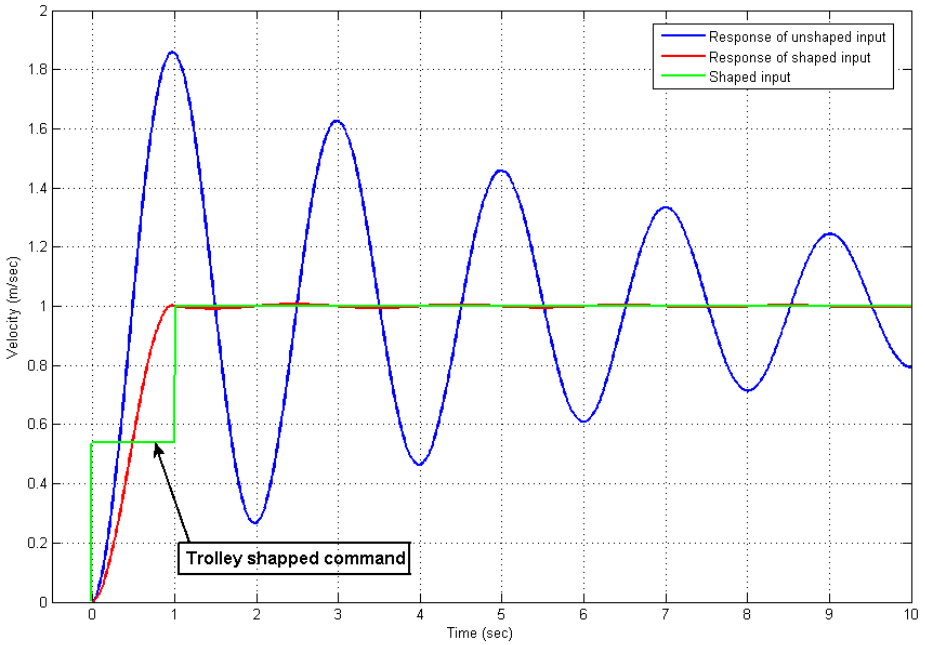

Figure 1-4 Shaped versus unshaped responses of a lightly damped second order system

1.2. INPUT SHAPER OF A LIGHTLY DAMPED SECOND ORDER SYSTEM

Many systems can be approximated as a cascade of second order systems. The following derivation is for a typical trolley gantry crane, schematic of which is shown in Fig. 1-5. The transfer function relating the payload angular deflection to the trolley velocity is:

$$\frac{\Theta(s)}{\dot{x}(s)} = \frac{\left(\omega_n^2 / g\right)(s)}{s^2 + 2\zeta\omega_n s + \omega_n^2} \qquad 1\text{-}1$$

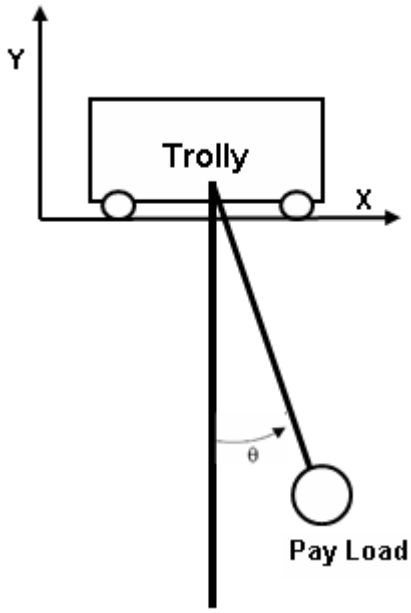

Figure 1-5 Schematic sketch of a trolley gantry crane

The response of this system to an impulse input is:

$$\Theta(t) = \left[\frac{A_0\omega_n}{\sqrt{1-\zeta^2}} e^{-\zeta\omega_n(t-t_0)}\right] \sin\left(\omega_n\sqrt{1-\zeta^2}(t-t_0)\right) \qquad 1\text{-}2$$

where ω_n is the natural frequency, ζ is the damping ratio, A_0 and t_0 are the impulse amplitude and timing respectively. Since the system is linear, the response for a set of impulses delayed in time is a superposition of equation 1-2:

$$\Theta(t)_{total} = \sum_{i=1}^{n}\left[\frac{A_i\omega_n}{\sqrt{1-\zeta^2}}e^{-\zeta\omega_n(t-t_i)}\right]\sin\left(\omega_n\sqrt{1-\zeta^2}(t-t_i)\right) \qquad 1\text{-}3$$

Where n is the total number of impulses, A_i and t_i are the amplitudes and timing of the i^{th} impulse. From equation (1-3) the amplitude of the vibration at the time of the last impulse can be evaluated as follows:

$$\Theta_{amplitude} = \frac{\omega_n}{\sqrt{1-\zeta^2}}e^{-\zeta\omega_n t_n}\sqrt{\left[C(\omega,\zeta)\right]^2+\left[S(\omega,\zeta)\right]^2} \qquad 1\text{-}4$$

Where, $C(\omega,\zeta)=\sum_{i=1}^{n}A_i e^{\zeta\omega t_i}\cos(\omega_d t_i)$, $S(\omega,\zeta)=\sum_{i=1}^{n}A_i e^{\zeta\omega t_i}\sin(\omega_d t_i)$

$$\omega_d = \omega_n\sqrt{1-\zeta^2}$$

The vibration level at the end of the impulse series expressed in percentage of unity impulse at t=0 is:

$$\theta_{\%\ residual} = e^{-\zeta\omega_n t_n}\sqrt{\left[C(\omega,\zeta)\right]^2+\left[S(\omega,\zeta)\right]^2} \qquad 1\text{-}5$$

For the residual vibration to cancel out after the second impulse both the sine and cosine terms has to sum to zero independently [3]. These constraints can be expressed in two equations and solved for the amplitude and timing of the impulses as follows.

$$\sum_{i=1}^{n}A_i e^{-\zeta\omega_n t_i}\cos(\omega_d t_i)=0 \qquad 1\text{-}6$$

$$\sum_{i=1}^{n}A_i e^{-\zeta\omega_n t_i}\sin(\omega_d t_i)=0 \qquad 1\text{-}7$$

For a given system both ω_n and ζ are known, equations 1-6, and 1-7 can be set to zero using n = 2 (two impulses). In this case there are four unknowns, namely A_1, t_1, A_2, t_2, where A_1 is the amplitude of the first impulse, and A_2 is the amplitude of the second impulse. While t_1, t_2 are the time delays of the first and second impulses respectively. Since, these two impulses should be convolved with the reference command to generate the shaped input, the amplitudes A_1 and A_2 have to sum to 1. Otherwise, the input shaper pre-filter would result in scaling of the input. This gives rise to one additional equation.

$$A_1 + A_2 = 1 \qquad 1\text{-}8$$

Equations 1-6 through 1-8 are three equations in four unknowns. The last unknown can be chosen to shorten the length of the shaping command by taking the first impulse timing at zero $t_1 = 0$. Using this information the impulses timings and amplitudes can be solved for in closed form as follows.

$$t_1 = 0 \qquad t_2 = \frac{\pi}{\omega_d} \qquad 1\text{-}9$$

$$A_1 = \frac{1}{1+\exp\left(\frac{-\zeta\pi}{\sqrt{1-\zeta^2}}\right)} \qquad A_2 = 1 - A_1 \qquad 1\text{-}10$$

Equations 1-9, 1-10 are the parameters fed to the input shaper in order to produce the self destructive response shown earlier in Fig. 1-4.

1.3. MOTIVATION

Since the introduction of input shaping in a formal way in 1990 [1], the research focus has been on improving input shaping theory and methodology. Creative and intensive research has been conducted in improving the robustness, adding motion constraints, and incorporating the nonlinearities in the design of the shapers.

However, there is currently a gap in the application of input shaping to new models in addition to the well-established cart-pendulum system. Input shaping is an effective method suitable to the motion control of other flexible system.

A traditional problem faced in production lines is the moving of open liquid containers. The sloshing of the liquid in open containers limits the speed of movement and waste time waiting for the liquid sloshing to die out. This problem is repeatedly faced in food industry as well as molten metal casting [4]. The work done in this thesis focuses on applying input shaping technique to mitigate liquid sloshing in open moving containers.

1.4. Objective and Approach

As stated above, the objective of this work is to develop a methodology for applying input shaping to the motion of an open container in order to limit the sloshing of the liquid inside. The approach followed is summarized below.

1- A numerical model is developed for both the driving motor and the liquid contained in a tank. The liquid is modeled using finite element analysis, and the time response is obtained by numerical integration of a set of ordinary differential equations. Unlike mathematical models, numerical models can capture irregular systems, and incorporate nonlinearities, similar to the work done in [5].

2- Since the sloshing liquid is a continuous system, the resulting vibration is expected to be multimodal. Instead of solving for the input shaper parameters in closed-form, the shaper is designed by optimization, i.e. to find the optimum commands that would result in the minimum amount of residual vibration. Other objectives and motion constraints can also be included in the optimization.

3- An experimental setup is built to verify the numerical models and the results obtained by optimization.

1.5. LITERATURE REVIEW

The idea of input shaping was first mentioned in the literature in 1958 by O.J.M. Smith [6] who introduced the technique of posicast control in which the reference step command is broken into two smaller steps that cancel out. However, the problem with this technique remained the robustness, since no feedback was involved. Singer and Seering [1] wrote a seminal work in 1990 where they introduced input shaping in a formal way for the first time and improved the robustness for parameter variations by introducing the concept of zero-vibration-derivative (ZVD) input shaping.

Since 1990 the research conducted in input shaping can be grouped into four main groups. 1- Improving the insensitivity by increasing the robustness of the shaper. 2- Including the effect of nonlinearities in the shaper design. 3- Hybridization of input shaping with other control techniques. Finally, 4- Applying input shaping to novel systems and models.

1.5.1. INPUT SHAPING ROBUSTNESS

The input shaping technique can be regarded as a finite impulse response (FIR)

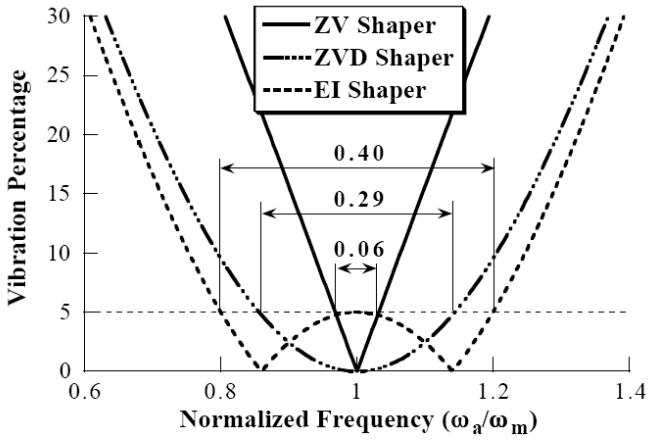

Figure 1-6 Comparison of the sensitivity of different input shapers to errors in ω_n [3]

filter. The open-loop nature of input shaping behaves poorly in case of modeling errors or system parameters variation. The first work done to improve the robustness of input shaping has been done by Singer and Seering [1]. They added the derivative of the residual vibration with respect to the sensitive system parameters as an additional constraint and set it to zero to get an insensitive filter, at the cost of increasing the rise time. They showed that input shaping performance is insensitive to variations in the damping ratio, but highly sensitive to variations in the natural frequency. Their work was continued by Singhose *et al.* [7] who made significant contributions in improving input shaping robustness. They showed that a broader range of tolerable variation in the parameters can be achieved if the zero vibration constraint is relaxed to a larger value. On the root locus plot this has the effect of adding two zeros around the flexible pole rather than on the pole as in the case of zero-vibration-derivative input shaper. The improvement of the shaper sensitivity came at no additional cost in the rise time. The new shaper was called extra-insensitive (EI) shaper. The EI effect is shown in Fig. 1-6 where the x axis is the actual over the modeled natural frequencies. In [8] Singhose *et al.* made the insensitivity to modeling error a design parameter by introducing a procedure that would solve for the shaper parameters given a pre-specified level of insensitivity. This shaper was named specified insensitivity (SI) input shaper.

Rather than improving the insensitivity in the direct feedforward direction, another technique is to use feedback to change the parameters of the input shaper in response to changes in the system parameters. This is known as adaptive input shaping. However, its practicality remains questionable since the feedback required in this case might not be applicable. In [9] Cutforth and Pao applied simple learning rule

to tune the parameters of the shaper in between and during maneuvers. The sensitivity curve and the phase shift curve were both used to determine the range of the modeling errors and tune the parameters accordingly. Other adaptive techniques may be found in [10,11].

1.5.2. Input Shaping for Nonlinear Systems:

The strength of input shaping technique is the straightforwardness and ease of application. This is true in case of simple linear systems. However, complications arise for nonlinear systems. The effect of nonlinearity is the subject of ongoing research, since nonlinearities limit the effectiveness of applying input shaping to real-life systems. In their work [12] Sorensen and Singhose discussed the effect of four hard nonlinearities on the performance of the input shaping, namely saturation, rate limiting, backlash and dead zone. They proposed some measures to quantify the detrimental effect of these nonlinearities on the residual vibration reduction of the linear input shapers. They also proposed a simple mitigation technique to reduce the effect of the nonlinearities. For the case of saturation and rate limiting the reference command is altered such that it remains within the saturation and the rate limit of the system before being fed to the input shaper filter. In this way the shaper itself will act in the linear zone and avoid the hard nonlinearities. For the case of backlash and dead zone they suggested the use of their inverse functions. Lawrence *et al.* provided a closed-form solution to systems with coulomb friction in [13], while in [5] Meshreki

provided a numerical optimization solution to a similar problem with both friction and motor saturation nonlinearities for two degrees of freedom system[1].

1.5.3. INPUT SHAPING HYBRIDIZATION

Many researchers have realized that the effectiveness of input shaping can be increased if it is combined with other control techniques that depend on feedback. Mohamed and Tokhi combined input shaping with time delay in [14]. They exploited the input shaping to filter out the flexible modes from the reference command to reduce the largest portion of the vibration, while switching to time delay at the end of the movement to suppress the remaining residual vibration and attain high positioning accuracy. Time delay is an alternative technique for reducing the vibration in flexible systems that is characterized by feeding back the position signal of the flexible mode delayed in time. This has the effect of adding more damping to the closed loop system. The feedback is expected to increase the insensitivity of the controller. Sorensen on the other hand exploited feedback for disturbance rejection. In his work [15] Sorensen *et al.* isolated the vibration due to any disturbance coming from outside the loop by comparing the actual response of the system to the input shaper command with the response from the mathematical model of the system to the same command. The difference between the two is the vibration due to outer disturbance. They applied a PD controller to suppress this disturbance and absorb the resulting energy in the

[1] The approach presented in this thesis is similar to the one adopted in [5]. In his work, Meshreki made use of Genetic algorithms to find the optimum input commands based on numerical integration of the system's states. He included the effect of nonlinearities inside the integration scheme.

flexible mode. They also added an additional loop for accurate positioning. The work of Meshreki in [5] also addressed the behavior of input shaping with both PD and PI controllers in order to attain high positioning accuracy in addition to suppressing the residual vibration by the input shaper.

1.5.4. Applications of Input Shaping

Input shaping was developed primarily for suppressing residual vibrations in cranes. The crane model was extensively studied in literature, while less attention was granted for other applications. Banerjee developed input shapers for satellite antennas in [16]. Such antennas suffer from high strain in response to satellite movements, which shortens their life time or in sever cases damages the structure. A numerical experiment was conducted whereby it was proved that input shaping is successful in reducing residual vibration and easy to implement. Singhose *et al.* extended the work of Banerjee by adding a deflection limiting constraint to limit the maximum deflection of the antenna during the entire motion, rather than at the end of the movement only [17]. Kojima and Singhose [11] recently showed that the deflection limiting input shaper can be made adaptive by evaluating the second natural frequency of the antenna online during motion, and use it to estimate the first natural frequency and determine the timing of the shaper impulses in real time.

A close variation of the antenna model is the case of a moving cart carrying an upright beam with concentrated mass at its tip addressed in [18]. This application is suitable for robot manipulators in production lines, for this purpose the authors added a robust internal loop compensator to achieve accurate point to point positioning.

In spite of the need for controlling the sloshing of fluids inside moving containers, this application has been poorly addressed in literature. Terashima and Yano [4]

applied input shaping to reduce the molten metal sloshing in metal casting production line. In this specific application an automatic tilting pouring machine pours the molten metal into one mold then tilts backward to wait for the next mold to be positioned correctly. The backward tilting movement causes sloshing of the molten metal inside, which limits the cycle time of the line. The fluid inside is modeled by two methods, one by using a representative pendulum-damper mechanical model, the other by using complex numerical simulation based on distributed parameter model. Input pre-shaping was applied for the angular tilting and compared with the original sinusoidal path function. It was shown that the input shaping outperforms the original system, and decreases the cycle time. An optimal control law was added to compensate for the control performance of the input shaper in response to the reduction of the system natural frequency of vibration, due to the reduction in the fluid level. However, in the discussion they provided, the practicality of the feedback loop was questioned because of the difficulty in sensing the molten metal level in real time. Therefore, it was recommended the study of the robustness of the shaper to changes in liquid level as well as the effect of the higher modes which were not captured in the simple mechanical model, or in the shaper design. The practical limitation of the sensors favors the open loop input shaper method for this application.

Feddema *et al*. also addressed sloshing suppression in moving tanks by input shaping in [19], where the focus was placed on applications with robot arm movements. The acceleration profile of the robot arm was based on the pendulum mechanical model. However, a double pendulum model was adopted for the case of slosh-free movement. In some applications such as in molten metal it is preferable to keep the fluid level from moving relative to the container in order to preserve the thin

film on the fluid surface. The authors made use of a second degree of freedom where the tank can be tilted around its axis during the translational movement.

1.6. THESIS OUTLINE

This thesis is organized into 5 Chapters. Chapter 2 presents the numerical models of the various components of the system under investigation. The detailed experimental setup is described in Chapter 3, followed by design and optimization of the input shapers as applied to the slosh suppression problem in Chapter 4. Experimental results are then compared to their numerical counterparts, and finally concluding remarks and future work are presented in Chapter 5.

CHAPTER 2

NUMERICAL MODELING

This Chapter presents the numerical modeling techniques adopted to simulate the dynamic behavior of the liquid tank under investigation, together with the actuating motor, in order to derive the complete differential equations governing the motion. These equations will then be numerically integrated to solve for the liquid behavior for various excitation schemes.

Section 1 explains the abstract block diagram of the system adopted and lists the advantages of the numerical model over the closed-form mathematical model. The system is decomposed in two separate models namely motor and tank. The motor dynamic numerical model is addressed in section 2, while, the water tank dynamic model is addressed in section 3. The two models developed are then combined into one integrated numerical model that represents the block diagram explained in the first section.

2.1. MODEL BLOCK DIAGRAM

Figure 2-1 shows a schematic diagram of the liquid tank under investigation. The tank is mounted on a motor-driven cart that is precisely guided to move along the horizontal direction. A detailed description of the experimental setup, together with the implemented sensors and actuators is presented in Chapter 3.

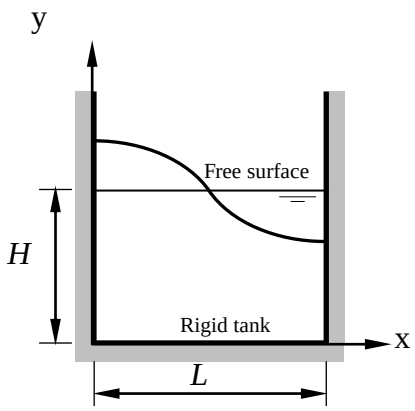

Figure 2-1 Schematic diagram of cart/tank system under investigation

Figure 2-2 shows a block diagram of the model adopted in the following chapters. This block diagram shows the mathematical relations between the different components of the system.

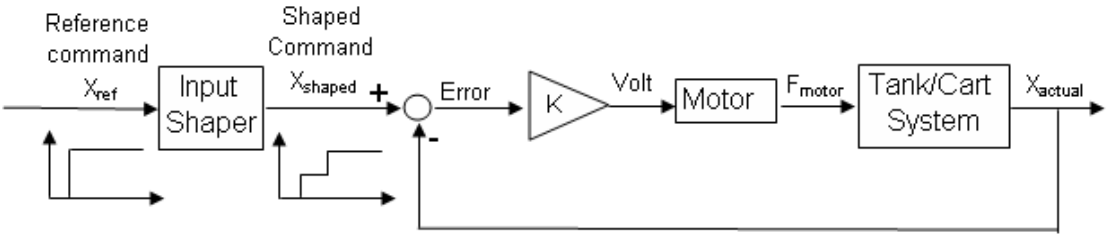

Figure 2-2 Tank/Cart/Motor numerical model block diagram

The input shaper block is responsible for changing the reference command into a shaped command that is designed to filter out the largest portion of the flexible modes of the system. The reference command can either be a velocity or a position signal. The reference command applied in this work is a step position signal. However, because the input shaper impulses are convolved with the reference command in real time, the shaper can work on any type of signal. The filtered shaped command is compared with the actual position of the cart, and the error signal is fed to a proportional controller, which simply multiplies the error by a constant gain. The

controller output signal is a voltage which is fed to a DC motor, whose force depends on both the input voltage and the back emf. The force applied by the motor acts on the cart carrying a tank filled with water. The resultant movement of the cart is affected by the fluid sloshing force inside the tank in addition to the force applied by the motor.

For the purpose of modeling the system represented by the block diagram shown in Fig. 2-2 above, the actions of each of the physical components are described by a set of first order differential equations. These equations are integrated numerically using Runge Kutta (RK)[1] scheme to solve for the system response. There are mainly two advantages that favor the numerical modeling over closed form mathematical solutions.

1-The inclusion of nonlinearities: Meshreki [5] showed that soft nonlinearities such as static and dynamic friction are hard to solve for in closed form, while hard nonlinearities such as motor saturation have no closed form solution. Saturation and other sorts of nonlinearities have significant effect on the system response. In fact, in practical applications they cannot be neglected. Building a numerical rather than a mathematical model of the system enables easy incorporation of these nonlinearities in the integration scheme, which produces more realistic response, as proved by the experimental results presented in the next Chapter.

2-Fluid sloshing modeling: fluid sloshing is a complex phenomenon. It has been thoroughly studied in the literature. Early simulations relied on building equivalent

[1] Fifth order adaptive Runge-Kutta scheme using Matlabe® (Mathworks Inc.) ode45 subroutine.

mechanical models. While these models provide a good reference for comparison and validation, they have limited modeling capabilities. For example, modeling of irregular shaped tanks or tanks with baffles is prohibitively complex. Also, as will be shown in the following section, mechanical models equivalence is based on fluid forces rather than fluid displacement, which dose not serve the objective of this research. Therefore, the fluid model adopted in the current work is a finite element model. In [20] Arafa presented a finite element model that handles the dynamics of rigid rectangular liquid tanks. This method is used and incorporated in the integration scheme as set of ordinary first order differential equations, to calculate the fluid response (both forces and displacement) for an arbitrary cart motion as will be shown in section 2.3.

2.2. MOTOR DYNAMIC MODELING

In this section the DC motor and cart governing equations will be derived. The equations will be arranged in state space format and the time response is calculated by RK integration. Two kinds of nonlinearities are incorporated, namely friction (both static and dynamic) and saturation. The results shown in this section are for the numerical model before parameter tuning (please refer to Chapter 3 for further details). Some parameters in the model will be tuned to match the real system. More results will be presented to compare the numerical model with the actual system.

The governing equation of the DC motor relates the applied voltage to the armature current and its rotation speed [21].

$$V = I_m R_m + K_m K_g \omega = I_m R_m + K_m K_g \frac{\dot{x}}{r} \qquad 2\text{-}1$$

where R_m, K_m, K_g are all motor constants, I_m is the armature current, ω is the motor rotational speed, r is the output gear radius $\dot{x}$ is the linear speed.

The torque and linear force produced by the motor are given by

$$T = K_m K_g I_m = F\, r \qquad 2\text{-}2$$

Equations 2-1, 2-2 can be grouped to express the resultant motor force as a function of the applied voltage and the motor/cart linear velocity.

$$F = \frac{K_m K_g}{Rr} V - \frac{K_m^2 K_g^2}{Rr^2} \dot{x} \qquad 2\text{-}3$$

The term $\frac{K_m K_g}{Rr}$ will be referred to as C_1, while C_2 will refer to $\frac{K_m^2 K_g^2}{Rr^2}$. The motor force accelerates the cart according to Newton's second law

$$F = M_{cart} \ddot{x} \qquad 2\text{-}4$$

Equations 2-3, 2-4 can be arranged in state space format by choosing the states as follows, $x_1 = x$, $x_2 = \dot{x}$. Two first order differential equations can be used to describe the dynamic behavior of the motor

$$\begin{aligned} \dot{x}_1 &= x_2 \\ \dot{x}_2 &= \left(\frac{C_1 V - C_2 x_2}{M_{cart}} \right) \end{aligned} \qquad 2\text{-}5$$

Equations 2-5 are both linear. Dynamic friction nonlinearity can be simply added as follows

$$\dot{x}_2 = \left(\frac{C_1 V - C_2 x_2 - \mu_k N \ sign(x_2)}{M_{cart}} \right) \qquad 2\text{-}6$$

where μ_k is the dynamic friction coefficient, N is the reaction force. Static friction can be added as a condition inside the numerical integration scheme where both velocity and acceleration are set to zero once the motor applied force is less than the static friction and the cart velocity is less than threshold value. The saturation nonlinearity is represented by a condition of scaling down the voltage to ± 5 volts. The above procedure is similar to the work done in [5]. The values of the physical experimental setup parameters are shown in appendix B.

It is worth mentioning that the above equations simulate the open loop behavior. The closed loop action will be addressed in section 2.4 where a complete representation of the block diagram in Fig. 2.2 will be discussed.

2.3. TANK SLOSHING MODELING

In this section both the mechanical and finite element models of a liquid sloshing inside partially filled tanks are presented. The mechanical model representation follows the work of [22] while the finite element model is based on the work done by [20]. Because of the reasons mentioned in section 2.1 the finite element model is the one adopted throughout the rest of this thesis.

2.3.1. SLOSHING MECHANICAL MODEL

A review of the pertinent literature reveals that a wealth of research has been expended to model sloshing phenomena in containers. The derivation of the governing equations for rectangular tanks from fluid dynamics principles is rather lengthy and beyond the scope of this work. Emphasis, however, will be placed primarily on those established equations that serve the current research objectives. For more detailed treatments of the subject, the reader is referred to the work of

Abramson [22] and to the more recent text by Ibrahim [23] which covers the dynamics of sloshing comprehensively.

The basic equations that describe the fluid sloshing is derived from velocity potential and based on the assumption that the fluid is inviscid and incompressible. The behavior of the liquid can be represented by mechanical components such as springs and masses, or pendulum as shown in Fig. 2-2. Mechanical models are built according to the following conditions [22]:

1- The equivalent masses and moments of inertia must be preserved.
2- The center of gravity must remain the same for small oscillations.
3- The system must possess the same modes of oscillations and produce the same damping forces.
4- The force and moment components under certain excitation must be equivalent to that produced by the actual system.

It is evident that mechanical models are not designed to predict the liquid free surface oscillations amplitude.

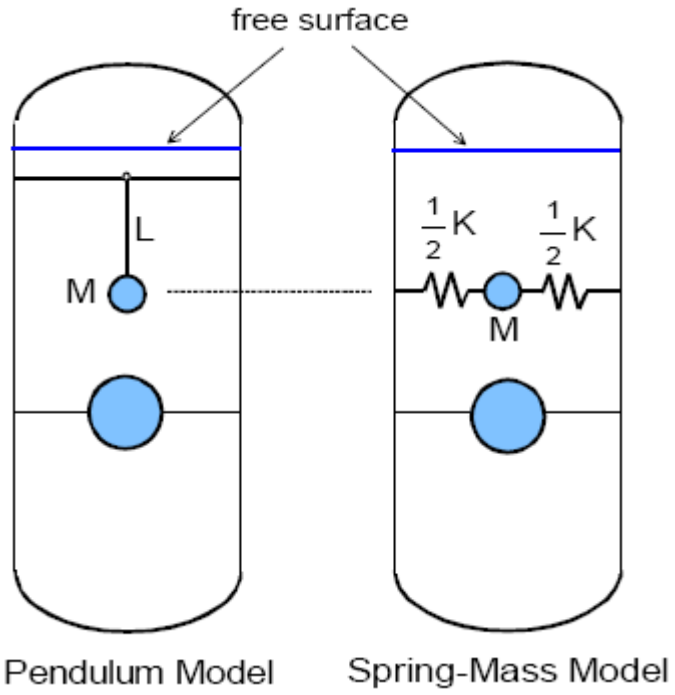

Figure 2-3 Equivelant Mechanical Models

The model shown in the Fig. 2-3 simulates the first mode of vibration only. Additional springs and masses can be added to simulate higher modes.

The natural frequencies of oscillation for rectangular tanks depend on liquid height and the tank dimension as described by equation 2-6

$$\omega_n^2 = (2n-1)\pi(g/a)\tanh\left[\pi(2n-1)(h/a)\right] \qquad 2\text{-}7$$

where h is the liquid height inside the tank, a is the tank other dimension, g is the acceleration of gravity and n is the n^{th} mode of vibration.

The mass M of the spring mass equivalent system shown in Fig 2-2 can be found by applying the 4 conditions of the mechanical models.

$$m_n = m_{liq}\left\{8\left(\frac{a}{h}\right)\frac{\tanh\left[(2n-1)\pi h/a\right]}{(2n-1)^3\pi^3}\right\} \qquad 2\text{-}8$$

where m_n is the mass representing the n^{th} node, and m_{liq} is the total liquid mass. Using 2-8 the spring stiffness can be solved for to satisfy the natural frequency in 2-7.

Equations 2-6 through 2-8 describe the sloshing of a liquid inside a moving tank in the light of the four conditions mentioned above.

$$K_n = m_{liq}\left\{8\left(\frac{g}{h}\right)\frac{\tanh^2\left[(2n-1)\pi h/A\right]}{(2n-1)^2\pi^2}\right\} \qquad 2\text{-}9$$

As a closed form solution the mechanical model role in the current work scope is the validation of the finite element model by comparing the natural frequencies of the two models.

2.3.2. SLOSHING FINITE ELEMENT MODEL

The finite element (FE) model of the sloshing behavior in rigid rectangular tanks has been presented by Arafa in [20]. Similar to the previous sub-section only the equations pertaining to the scope of the current work will be mentioned.

In the FE model proposed by Arafa and adopted here, the liquid domain is discretized into two-dimensional four-node rectangular elements with the liquid velocity potential representing the nodal degrees of freedom. Liquid sloshing effects can be induced either by steady-state harmonic or arbitrary base excitation. The objective is to be able to determine the slosh frequencies, liquid velocity field, free surface displacement and hydrodynamic forces acting on the tank walls for various excitation schemes. Fluid—structure interaction is accounted for in the model to

couple the liquid motion with the rigid tank walls to ensure continuity of liquid and structural motion at the liquid—tank interface.

In order to include the rigid enclosure in the present finite element formulation, three spring-supported pistons are attached to the liquid domain, as depicted in Fig. 2-4. Mass and stiffness parameters of the additional mass—spring systems are selected to ensure the walls of the container are practically rigid and possess natural frequencies that are appreciably higher than the frequency range of interest which includes the liquid slosh frequencies.

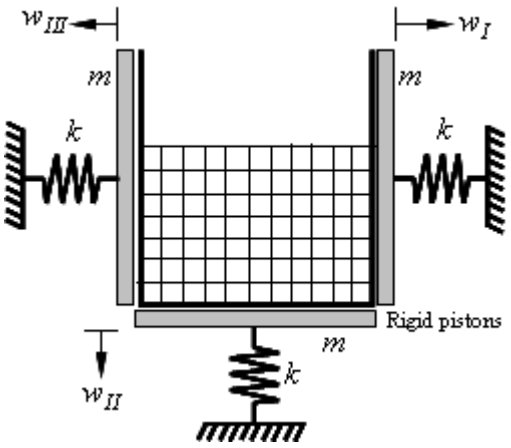

Figure 2-4 Modeling of the tank walls as rigid spring-supported pistons

The procedure of building the FE model is fairly simple. Starting from the basic equation of the velocity field of the fluid, and satisfying set of boundary conditions including the direction of the velocity at the wet-walls and continuity, expressions for the kinetic and potential energies of the elements can be derived. Applying Lagrange's equations gives the equation of motion governing the system. The coefficients of the equation of motion can be used as the mass and stiffness matrices of the FE model. The final FE equation of motion becomes.

$$\begin{bmatrix} [M_{ff}] & \{M_{12}\} & \{M_{13}\} & \{M_{14}\} \\ 0 & m_{22} & m_{23} & m_{24} \\ 0 & m_{32} & m_{33} & m_{34} \\ 0 & m_{42} & m_{43} & m_{44} \end{bmatrix} \begin{Bmatrix} \{\ddot{p}_f\} \\ \ddot{w}_I \\ \ddot{w}_{II} \\ \ddot{w}_{III} \end{Bmatrix} + \begin{bmatrix} [K_{11}] & 0 & 0 & 0 \\ \{K_{21}\} & \rho k & 0 & 0 \\ \{K_{31}\} & 0 & \rho k & 0 \\ \{K_{41}\} & 0 & 0 & \rho k \end{bmatrix} \begin{Bmatrix} \{p_f\} \\ w_I \\ w_{II} \\ w_{III} \end{Bmatrix} = \begin{Bmatrix} \{0\} \\ \rho f_I \\ \rho f_{II} \\ \rho f_{III} \end{Bmatrix} \quad 2\text{-}10$$

where ρ is the fluid density, k is the stiffness of the spring-supported pistons shown in Fig.2-4 and all other parameters denote coefficients in the mass and stiffness matrices. $w_{I\to III}, \ddot{w}_{I\to III}$ are the positions and accelerations of the tank walls respectively, following the notation and directions shown in Fig. 2-4. $p_f, \ddot{p}_f$ are the pressure and second derivative of the pressure with respect to time of the free fluid surface. Finally, $f_{I\to III}$ are the hydrodynamic forces applied by the fluid on the walls of the tank.

To validate the accuracy of the present FE formulation, the model is employed to study the sloshing characteristics of water having ρ=1000 kg/m^3 in a rigid rectangular tank having the dimensions of the tank available in the lab. The length L and width b are both taken to be 0.1 m and the filling height H is 0.04 m. The liquid region is divided into 20 by 20 elements. The liquid slosh frequencies are calculated and compared in Table 2.1 with the analytical values based on equation 2-7.

Inspection of the results reveals that the present FE formulation is quite accurate in predicting the slosh frequencies with a percentage error of about 1.5% up to the fifth mode. Higher frequencies can be predicted more precisely by increasing the number of elements, but on the expense of longer computational time, which is a typical trade-off in these types of problems. Since the FE model will later be incorporated in a rather computationally intensive optimization scheme, the present accuracy obtained with a 20 x 20 mesh is considered sufficient.

Table 2-1 Liquid slosh frequencies in a fixed tank (L = 0.1 m, H = 0.04 m, b = 0.1 m)

Mode	Natural frequencies [Hz]	
	Present	Analytical
1	2.5783	2.5762
2	3.9355	3.9255
3	4.8631	4.8368
4	5.6415	5.5878
5	6.3415	6.2476

Figure 2-5 shows the liquid velocity field at the first three slosh modes, as obtained from the present finite element analysis. Liquid particles adjacent to boundaries of the tank are shown to possess velocity vectors that are parallel to the boundary surfaces, in agreement with the boundary conditions imposed. It is worthy to note that only the odd modes will be excited during the horizontal tank motion, as shown by Abramson [22]. Damping can easily be incorporated into the model by introducing an artificial proportional damping matrix in the form $C = \zeta [K] \dot{P}_f$ in the equations of motion.

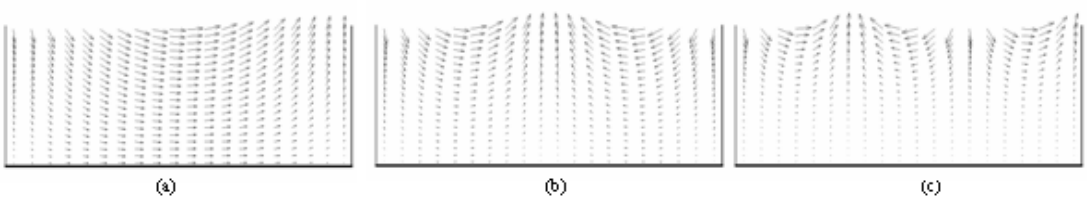

Figure 2-5 Liquid velocity field in the (a) first,(b) second and (c) third slosh mode

2.4. MOTOR/CART/TANK COMBINED MODEL

Equation 2-10 in its present format cannot be used to solve for the response of the liquid inside the tank while incorporating the closed loop motor model, and hence has to be manipulated and rearranged as shown below.

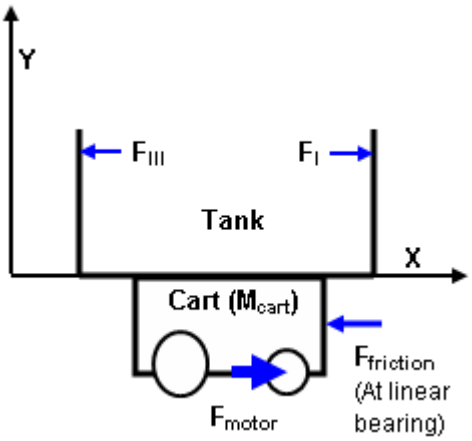

Figure 2-6 Schematic free body diagram of Tank/Motor/Cart system

Figure 2-6 shows a schematic free body diagram of the experimental cart/tank set-up explained in details in Chapter 3.

F_I and F_{III} are the hydrodynamic sloshing force applied by the liquid on the tank walls. The state space representation of this model can be expressed as follows,

$$x_1 = x,\ x_2 = \dot{x},\ x_{3\to n+3} = P_{f1\to n},\ x_{n+4\to 2n+4} = \dot{P}_{f1\to n} \qquad 2\text{-}6$$

Where n is the number of elements of the FE mesh, P_f is the pressure of the free surface. The first derivative of the states can be found using the free body diagram in Fig 2-5 and equations 2-6, and 2-10.

$$\dot{x}_1 = x_2 \qquad 2\text{-}12$$

$$M_{cart}\dot{x}_2 = f_I - f_{III} + F_{motor} - f_{friction} \qquad 2\text{-}13$$

$$M_{cart}\dot{x}_2 = \left[(m_{22} - m_{24} - m_{42} + m_{44})\dot{x}_2 + \{K_{21}\}\{x_{3\to n+3}\} - \{K_{41}\}\{x_{3\to n+3}\} \right] / \rho + F_{motor} - f_{friction} \quad \text{2-14}$$

where the tank wall acceleration $\ddot{w}_I, \ddot{w}_{III}$ in 2-10 are substituted for by the cart acceleration $\dot{x}_2$. It is worth mentioning that according to the directions shown in Fig. 2-3 $\ddot{w}_I = \dot{x}_2$, $\ddot{w}_{II} = 0$, and $\ddot{w}_{III} = -\dot{x}_2$. The unknown term in equation 2-14 can be collected on the left hand side as follows

$$\dot{x}_2 = \frac{\left[F_{motor} - f_{friction} + \{K_{21} - K_{41}\}\{x_{3\to n+3}\}/\rho\right]}{\left[\rho M_{cart} - m_{22} + m_{24} + m_{42} - m_{44}\right]/\rho} \quad \text{2-15}$$

Equations 2-12,2-15 are subject to the static friction condition stated previously in section 2-2.

The F_{motor} term can be found using equation 2-4, rewritten here in a state space format for completeness

$$F_{motor} = \frac{K_m K_g}{R \times r} V - \frac{K_m^2 K_g^2}{R \times r^2} x_2 \quad \text{2-3}$$

By examining the block diagram in Fig. 2-1 motor voltage can be expressed in the light of the closed loop system. Assuming the shaped signal is a step position signal x_d, where x_d changes with time according to the shaper parameters.

$$V = x_d - x_1, \text{ Subject to the saturation condition } -5 < V < 5 \quad \text{2-16}$$

Equations 2-10, 2-13 now define the cart dynamics including the sloshing effect of the fluid inside the tank. Equations 2-3, 2-16 define the motor dynamics after closing the loop. The fluid dynamics inside the tank are defined by the states representing the free surface pressure derived from the first row equation of 2-10, as follows

$$\dot{x}_{3\to n+3} = x_{n+4\to 2n+4} \qquad 2\text{-}17$$

$$\dot{x}_{n+4\to 2n+4} = \left(M_{ff}\right)^{-1}\left[\{M_{14} - M_{12}\}\dot{x}_2 - K_{11}x_{3\to n+3}\right] \qquad 2\text{-}18$$

where M_{ff}, K_{11} are the mass and stiffness matrices respectively. M_{14}, M_{12} are constants defined from the FE analysis. For the case of damped response, a damping coefficient proportional to the stiffness can be added as shown in equation 2-19

$$\dot{x}_{n+4\to 2n+4} = \left(M_{ff}\right)^{-1}\left[\{M_{14} - M_{12}\}\dot{x}_2 - K_{11}x_{3\to n+3} - \zeta K_{11}\dot{x}_{3\to 3+n}\right] \qquad 2\text{-}19$$

Once the free surface pressure P_f is determined the free surface displacement can be calculated easily by $U_i = \frac{P_{fi}}{\rho g}$, $i = 1 \to n$ where n is the number of elements in the mesh.

The states' first derivative equations 2-12, 2-15, 2-17 and 2-18 in addition to the closed loop motor dynamics equations 2-3, and 2-16 are the complete dynamic model for a system composed of a DC motor driving a cart that carries a tank partially filled with inviscid/incompressible fluid, represented by the block diagram in Fig 2-1. The time response of arbitrary position command is calculated by integrating the states' equation.

CHAPTER 3

EXPERIMENTAL WORK

The purpose of this Chapter is to document the experimental work carried out to validate the numerical model presented in Chapter 2, and the results obtained in the following chapters. The experimental model is based on a setup provided by Quanser [21]. It has gone through numerous modifications before reaching its final shape. Because of its fairly simple structure and small number of components the model proved to be sufficiently accurate and robust to serve the purpose and scope of this research work. Section 1 will explain the model built and the block diagram of the experiment. Section 2 will be dedicated for validation and comparison between the numerical model presented in chapter 2 and the experimental model. The fine tuning of the numerical model based on the results obtained from the experiment will also be discussed.

3.1. EXPERIMENTAL MODEL

Fig. 3-1 shows two views of the experimental setup with the components labeled below. The original setup provided by Quanser [21] is connected to a PC and controlled through Simulink. The real-time-workshop enables building controllers in Simulink, compiling the models, and transferring them to c-code that is downloadable to the microcontroller. The data collected by the sensors and encoders can be recorded and manipulated directly from within Matlab environment.

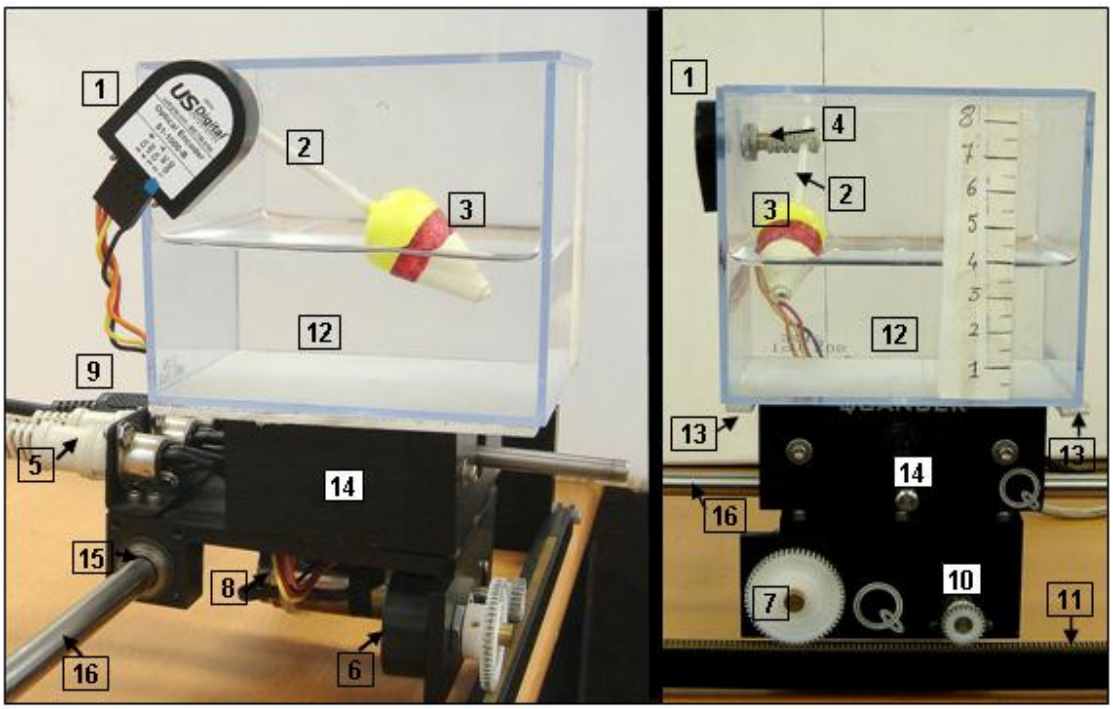

a) Side View b) Front View

Components Key:

1) Optical encoder for water level measurment.
2) Arm connecting the floating indicator to the encoder shaft.
3) Floating indicator of the water level.
4) Optical encoder shaft directly connected to the floating indicator arm.
5) Optical encoders' cables transfering data to the controlling PC.
6) Cart position optical encoder.
7) Position optical encoder shaft
8) DC motor.
9) Motor power cable (from the controlloing PC)
10) Motor pinion.
11) Rack.
12) Partially filled water tank (10x10x8) cm.
13) Guides to support the tank on the cart
14) Cart (housing for the motor and the tank).
15) Linear bearing.
16) Slider guides for the cart.

Figure 3-1 Experimental setup components

The setup consists of a cart carrying a DC motor. The cart slides with linear bearing on a smooth guide at the back side, while driven on a rack by the motor pinion at the front side. The position of the cart is sensed by an optical encoder

connected to the rack via gear. This basic setup is modified to suit the purpose of the current research work by adding a tank partially filled with water on top of the cart.

The dimensions of the tank are (10x10x8 cm). The tank is supported on the cart via plastic guides in order to prevent slippage. A block diagram of the experimental model is shown in Fig. 3-2. Note the way the zero vibration (ZV) input shaper is modeled (see Chapter 4). The step reference command is passed to two gain blocks namely A_1 and A_2. Those gain blocks represent the first and second amplitude of the shaper impulses. The signal passing through A_2 is delayed in time a value of T_2 before being added to the signal passing through A_1. The summation of the signals through A_1 and A_2 is the shaped command indicated by the shaped signal label. It is worth

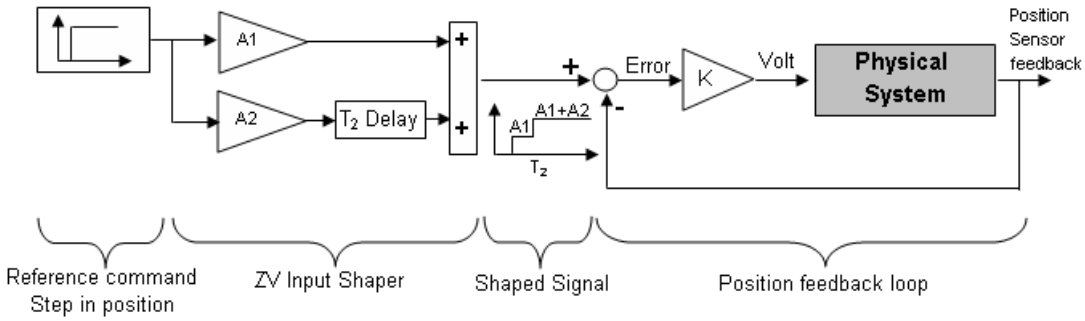

Figure 3-2 Experimental Model Block Diagram

mentioning that the parameters of the ZV input shaper as presented here are A_1 and T_2 only, since A_1 and A_2 has to sum up to unity as stated in chapter 1, and T_1 (delay of the first impulse) is chosen to be zero to reduce the shaper time.

3.1.1. WATER LEVEL MEASURING SENSOR

Although input shaping is a feedforward approach that does not require feeding back the control variable (water level in this case), the control variable still had to be measured for analysis, validation, and comparison purposes. Otherwise, the results

would have been all reported qualitatively. Measuring water level in real time on a moving cart proved to be a challenging task. The measuring device had to be chosen and mounted in a way that does not influence the dynamics of the system. It had also to measure the water level in real time and feed the data back to the PC for storage and analysis. Unfortunately, no non-contact sensor was capable of performing this task within satisfactory accuracy limits and budget as well.

The current contact sensor is an assembly of a floating indicator, connecting arm, and optical encoder mounted on the tank wall as shown in Fig. 3-1. Because the connecting arm is directly coupled to the shaft encoder, no slippage, friction, relative motion or backlash takes place. The floating indicator captures the water free surface displacement fairly accurately, especially in the low frequency range. When the motion turns into nonlinear or changes rapidly at high excitation frequencies, the floating indicator fails to follow the water surface. However, this kind of motion is outside the scope of work. The arm connecting the floating indicator to the encoder shaft turns the vertical displacement of the water free surface into rotary deflection at the shaft encoder. The encoder reads relative angular deflection. At the start of motion, when the water surface is level, the encoder reads zero degrees, as the cart moves and water surface is disturbed, the encoder reads the angular rotation of the connecting arm due to the vertical displacement of the water level. The rotation recorded by the encoder is related to the water surface relative displacement by a constant calibration factor. This is a valid approximation because the angles are all small compared to the connecting arm length. The sensitivities and calibration constants for both the water level, and position optical encoders are shown in Appendix A.

Although the water level measuring device is not expected to be perfectly accurate in the global sense, its repeatability is sufficient to ensure accuracy in the relative sense. This can be better understood in the light of Fig. 3-3.

The pyramid-like graph in Fig. 3-3 is the sensor readings in cm of water level. In the first portion, 0.5 cm of water is added at each step (measured by a scale). The reverse happens in the second portion, where 0.5 cm of water is taken away from the tank at each step. The final value recorded is around 1.86 cm while it should read 2 cm, this is an error of 7%. While this is relatively high error in the global sense, the maximum difference between the readings of two steps is only 0.06 cm, showing acceptable error in the relative sense. The pyramid shape of the forward and reverse runs suggests sufficient repeatability as well.

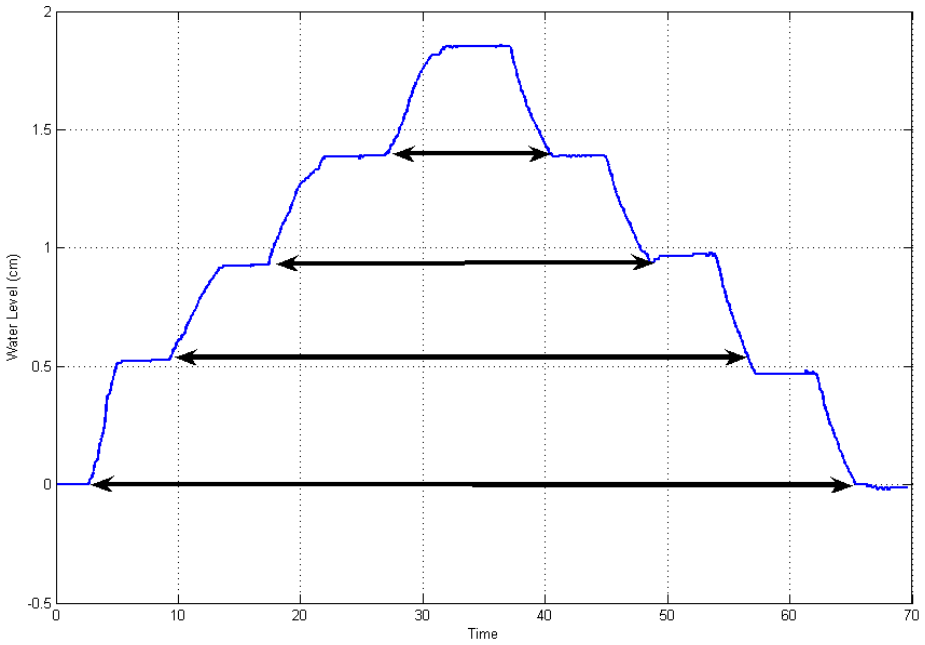

Figure 3-3 Water level measuring device accuracy and repeatability

Generally speaking, the setup accuracy and handling are adequate for the scope of this work.

3.2. NUMERICAL VS EXPERIMENTAL MODELS

The purpose of this section is to compare and fine tune the numerical model with the experimental runs. The procedure followed was first to tune the motor numerical model alone, then, to use the results obtained to tune the motor/cart/tank combined model. Some of the tuning parameters were solved for using the experimental data, such as the static and dynamic friction, others were found by trial-and-error such as motor constants and water damping. It is worth noting that more rigorous procedure could be employed to fine-tune the numerical model. The procedure could have involved multiple runs and design-of-experiment concepts. However, given the scope and objective of the work, in addition to the inaccuracies inherent in the experimental model itself, identical agreement between the numerical and experimental models is both unattainable and unnecessary. The purpose of the tuned-numerical model is to faithfully reflect the actual system behavior form, and to be repeatable and reliable in a relative sense rather than producing the same results of the experimental setup. For example, if certain shaper succeeds in suppressing 50% of the unshaped residual vibration amplitude, it is more crucial that the numerical model predicts this 50% accurately than to predict the actual values of residual vibration amplitudes in the shaped and unshaped runs. It will be shown in the following Chapter that the objective function of the optimization scheme depends on the relative performance and not the absolute performance.

3.2.1. MOTOR MODEL

There are four tunable parameters in the motor numerical model, namely C_1, C_2, static friction coefficient and dynamic friction coefficient. C_1, and C_2 are the volt and

back emf constants in equation 2-3 respectively. These constants are expected to be different from the values reported in the kit manual because the motor is subject to degradation. The actual values of these constants were determined by trial and error.

The static friction can be evaluated by applying voltage to the motor in small steps and recording the voltage at which the motor starts motion. The force applied by the motor at this point can be found using equation 2-4 and the static friction coefficient can be calculated. The dynamic friction coefficient was evaluated similar to the work done in [5] where the coefficient is the slope of the cart velocity versus motor voltage curve.

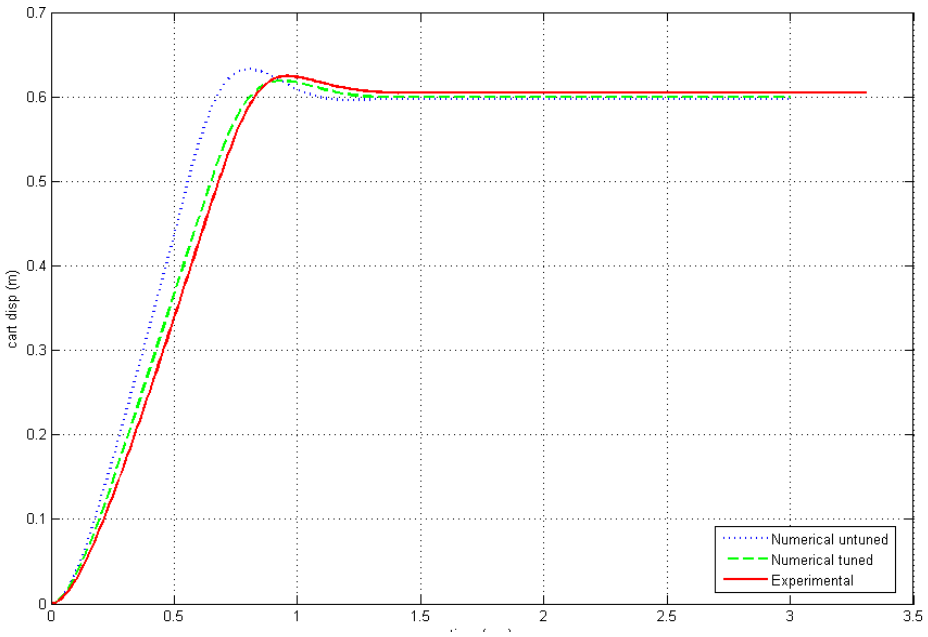

Figure 3-4 Numerical versus actual motor response

Fig. 3-4 shows a comparison between the numerical model response before and after tuning, and the experimental response. The adjustment of the back emf constant C_2 is responsible for the slope of the rising portion of the curve. The larger the value of C_2 the less steep the slope is. On the other hand, C_1 is responsible for the maximum overshoot reached. The larger the value of C_1 the higher the value of the maximum overshoot reached. To adjust the untuned numerical model shown in blue in Fig. 3-4

to respond similar to the experimental model shown in red, the reported value of C_1 was decreased by a factor of 10% while C_2 reported value was increased by 10%. The dynamic friction coefficient mildly affects both the maximum overshoot and the rising slope. Finally, the static friction affects the final value reached by the motor. The tuning factors and the rest of the physical parameters of the motor and cart are shown in Appendix A.

Because the position control loop is simple gain controller, the motor does not settle exactly at the desired final value, the presence of the static friction coefficient prevents the motor from reaching the desired position.

The graph shown in Fig. 3-4 is for controller gain of 25 and desired final value of 0.6m. Different scenarios of gain and desired positions were tried, but not shown for briefness. All runs showed close agreement between the numerical and experimental models.

3.2.2. SLOSHING MODEL

The tuned parameters of the motor numerical model are now integrated in the combined model described in section 2.4. The response of the numerical integration of the FE model combined with the motor and cart dynamics is shown in Fig. 3-5.

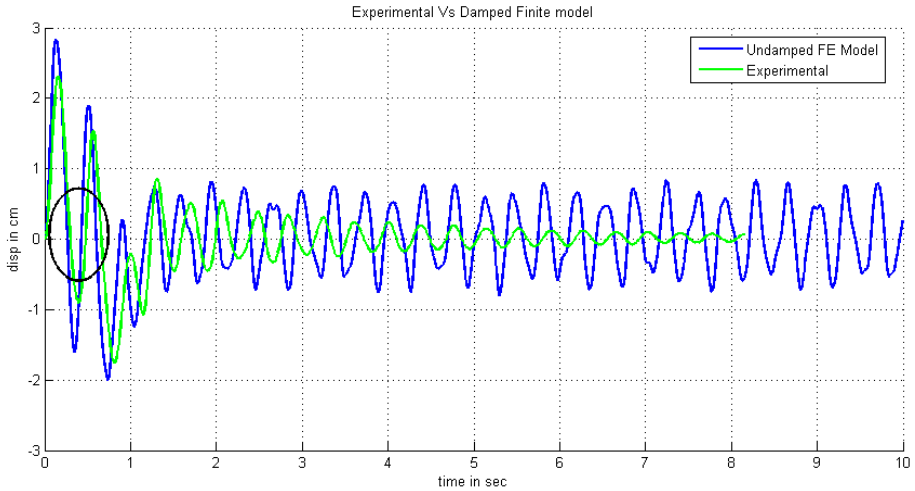

Figure 3-5 Undamped numerical model versus experimental data

The controller gain for the run in Fig. 3-5 is 25, the desired final position of the cart is 0.6m and the water height in the tank is 4cm. Clearly, Fig. 3-5 shows discrepancy between the two responses. However, some observations were useful to help building an improved model. The main source of discrepancy is the damping effect especially evident after the motor settles at 1.5 s

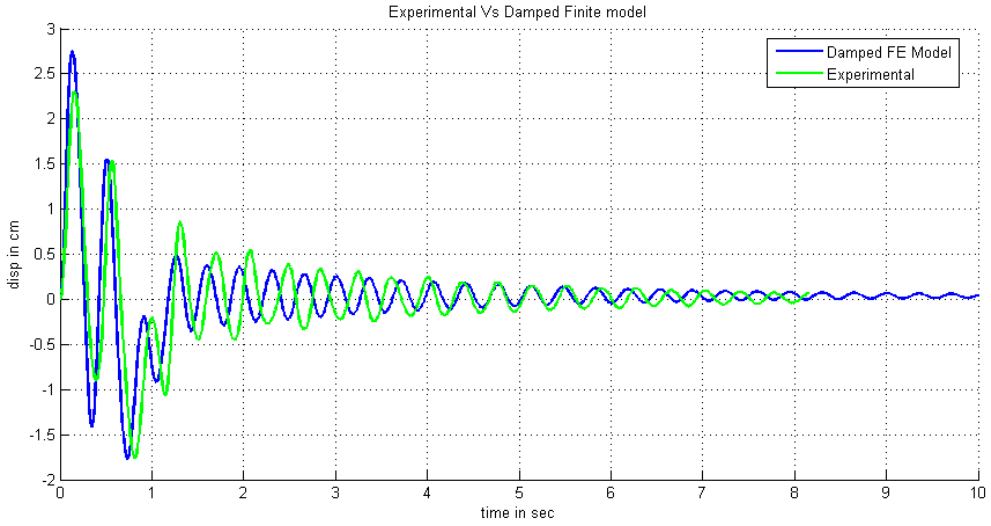

Figure 3-6 Damped numerical model versus experimental data

From the exponential shape of the decay curve, the type of damping is expected to be viscous damping, where the damping force is related to the velocity of the fluid particles.

The second source of discrepancy is the natural frequency of vibration. Although both the numerical and experimental responses have nearly an identical period time for the first two cycles (emphasized on the graph by the ellipse), errors in the frequency starts building up afterwards.

The first discrepancy was mitigated by adding a damping term proportional to the velocity of the FE nodes and the stiffness matrix. The value of the damping coefficient was adjusted by trial and error to be 0.0025 to match the experimental rate

of decay. On the other hand, the second observation may be attributed to nonlinearities due to the tank's small dimension, such as surface tension force and viscous effects. However these effects were neglected in the present study for simplicity. The modified model with the addition of damping proved to be sufficiently accurate for the purpose of this research. The results in Fig. 3-6 shows a close matching between the FE and experimental responses.

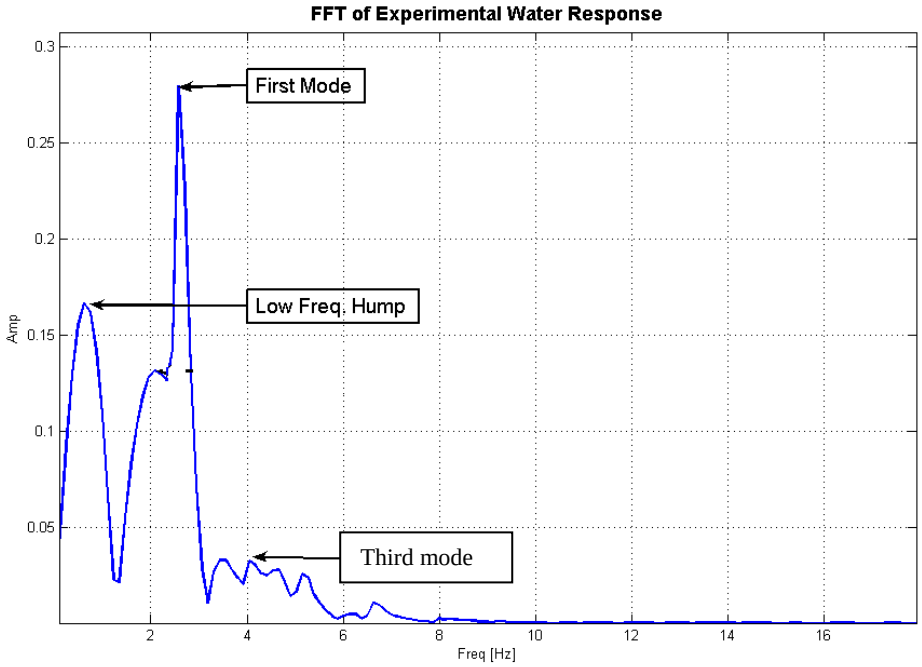

Figure 3.7 Frequency spectrum of the experimental data of the water level

More insight into the system is gained by examining the response spectrum by performing Fast Fourier Transform (FFT) of both the experimental and numerical model data.

Fig. 3-7, 3-8 shows the FFT spectrum for the experimental data and numerical model of the previous run respectively. Two remarks are worth mentioning concerning the FFT analysis. The Theoretical (closed-form solution) values of the first and second mode of vibration are 2.57 Hz and 3.93 Hz respectively.

The experimental data shows a distinct peak at the first mode at 2.576 coinciding with the theoretical value. The second mode peak is less distinct. It shows a range of frequencies from 3.6 up to 5 Hz. However the theoretical value of the second mode lies almost at the middle of the range.

The reason behind this close matching between theoretical experimental frequencies is that the frequency domain is less prone to sensors' errors, due to the summing nature of the transform that tends to cancel errors. The response spectrum of the FE numerical model in Fig. 3-8 is in very good agreement with the experimental results, which illustrates the model's credibility and reliability.

As indicated in Fig. 3-7, and Fig. 3-8, there is a peak at a frequency of around 0.66 Hz. This peak is unexplainable since it is lower than the first mode peak. It cannot be attributed to any experimental deficiencies either since it appears both in the experimental and numerical spectrum. The most reasonable explanation of this hump is the motor effect. When the motor starts motion at t = 0, the water inside the tank is subjected to a step excitation (from rest to motion), this excitation produces

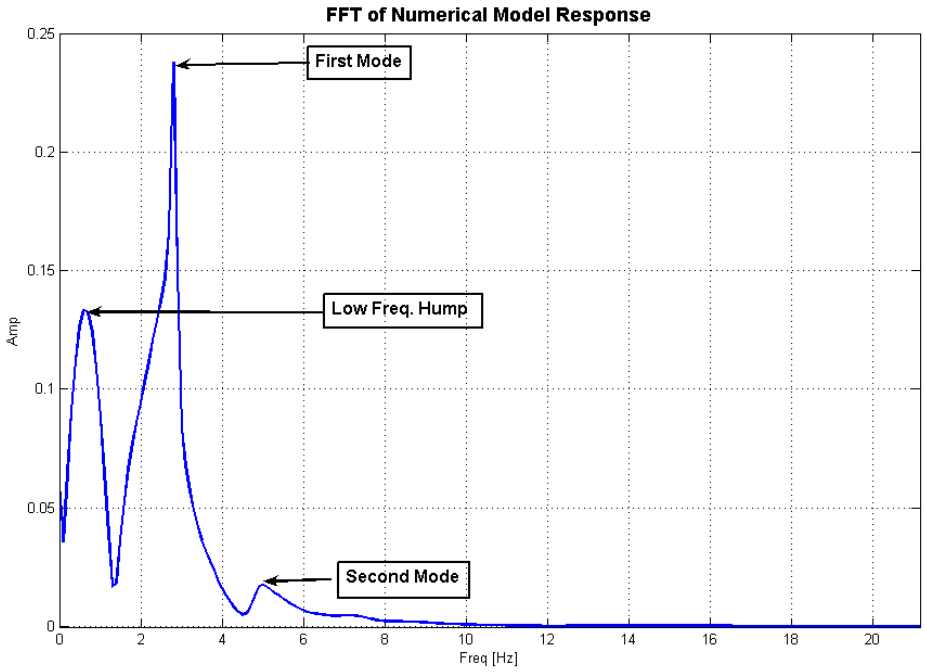

Figure 3.8 Frequency spectrum of the numerical model of the water level

certain response. When the motor stops motion at $t = t_s$ where t_s is the motor settling time, the water inside the tank is subjected to another step excitation (from motion to rest). This excitation is expected to produce the same response as the first excitation. In this case, the entire response of the water to the two step responses delayed in time can be considered a wave in itself, since essentially it is a signal repeating itself with certain time delay. This explanation is further supported by the fact that the motor settling time of the previous run is 1.5 s, which corresponds to a frequency of 0.66 Hz exactly. To further validate this explanation the experiment is repeated with the desired final position of the cart reduced to 0.4m instead of the 0.6m in the previous run, in order to reduce the settling time of the motor and examine the effect on the spectrum. The motor cart responses for 0.4m and 0.6m are shown in Fig. 3-9. In the case of 0.4m desired final position the motor settles in 1.15 s, while it settle in 1.5 s in the case of 0.6m. The spectrum of both runs is shown superimposed in Fig. 3-10. The low frequency shifts from 0.66 Hz in the first run to 0.88Hz in the second run, while the rest of spectrum remains essentially unchanged. The low frequency hump matches the motor settling time in both situations.

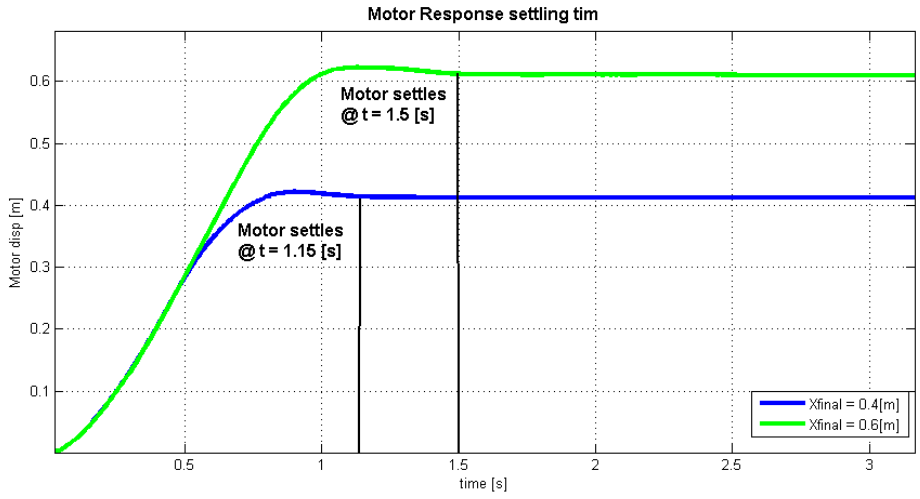

Figure 3-9 Experimental results of the motor response at desired final position of 0.6 and 0.4

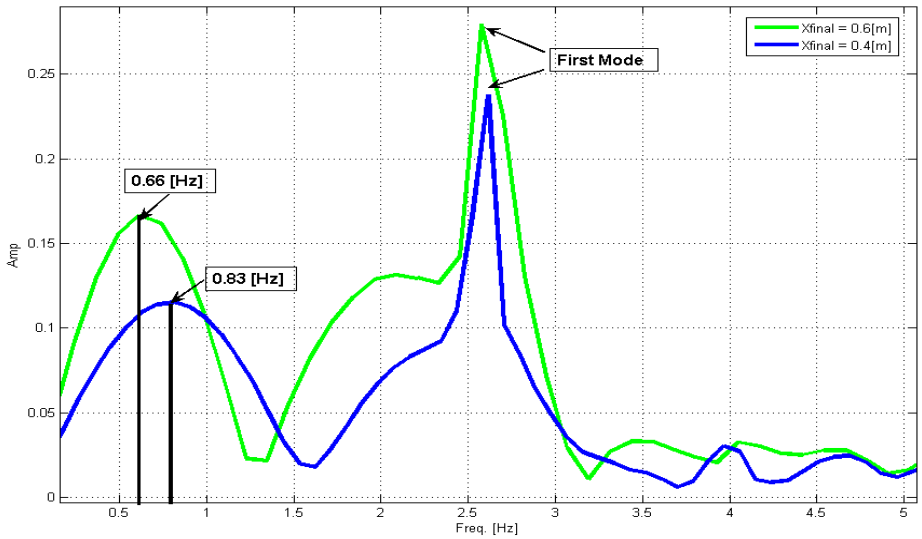

Figure 3-10 Frequency spectrum of the water level response at different final cart

CHAPTER 4

INPUT SHAPING DESIGN USING OPTIMIZATION

In the previous two chapters, both the numerical and experimental models were presented and validated. In this Chapter the numerical model will be used to supply an optimization scheme with the time response for a reference command prefiltered by an input shaper. The optimization variables will be the shaper parameters and the objective function will be based on the time response.

4.1. LINEAR INPUT SHAPER

As mentioned in Chapter 1, although input shaping design is a straightforward procedure in the case of linear systems, the presence of nonlinearities complicates this process. Theoretically speaking within certain limits sloshing can be regarded as a linear phenomenon. However, in this application, the coupling of the sloshing with the cart's movement and the nonlinearities inherent in the motor response precludes the trivial linear solution. To illustrate this concept practically, a zero vibration (ZV) input shaper is designed based on the first natural frequency following the procedure mentioned in section 1-2 using equations 1-9, 1-10. For the case of a water height of 4 cm the first natural frequency is 2.57 Hz. The linear shaper parameters are listed in Appendix C. The response of the water to this shaper is shown in Fig 4-1. This

response is identical to the unshaped case[1]. In other words the shaper failed to reduce, or even to affect the performance of the system. This failure is explained in [2] and is attributed to the motor nonlinearity.

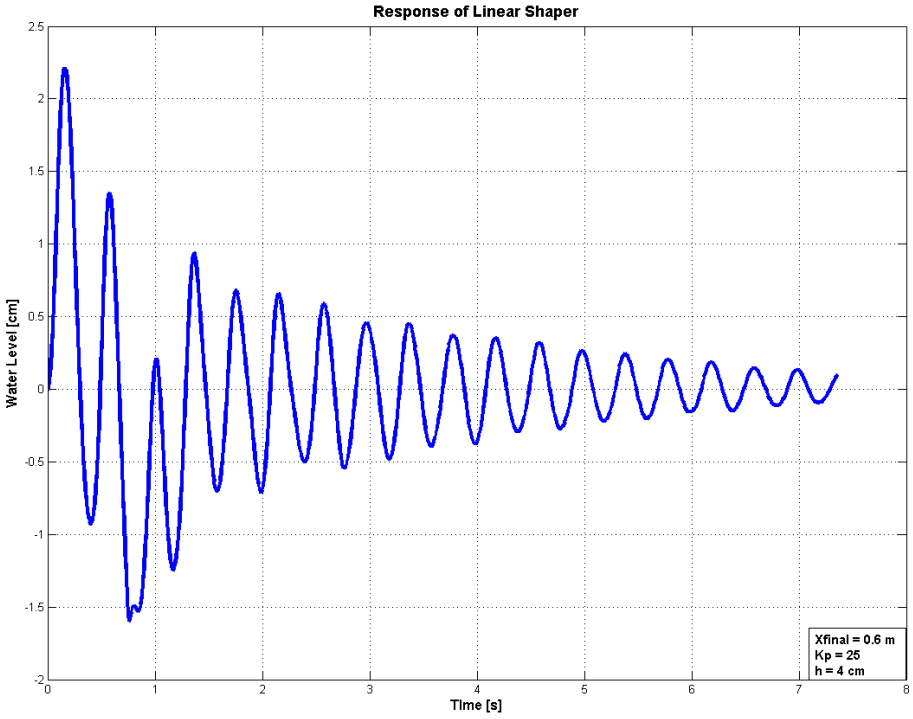

Figure 4.1 Experimental Response to linear shaper

The discussion in Sornesen [2] addressed the case when the control variable is the velocity. In such case the slew rate[2] of the motor affects the shaper performance. Fig 4-2 shows 8 motors responses with different values of slew rate, as well as the

[1] The unshaped response graph could not be superimposed on the linear shaper response for comparison because they are perfectly identical.

[2] Slew rate is a nonlinearity that describes the rate at which the motor responds to the changes in the applied velocity command. A theoretical motor with zero slew rate will have infinite acceleration response.

velocity shaper command. Sorensen showed that the acceptable slew rate range lies in the portion where the motor speed will reach the first desired speed value, 50% in this case, before the time of the second desired speed value. In simpler terms if the motor's response is slower than the ZV second impulse timing, the input shaper will not perform its function. In fact in this case the input shaper is expected to have minimal or no effect on the response, since it fails to follow the input shaper's commands.

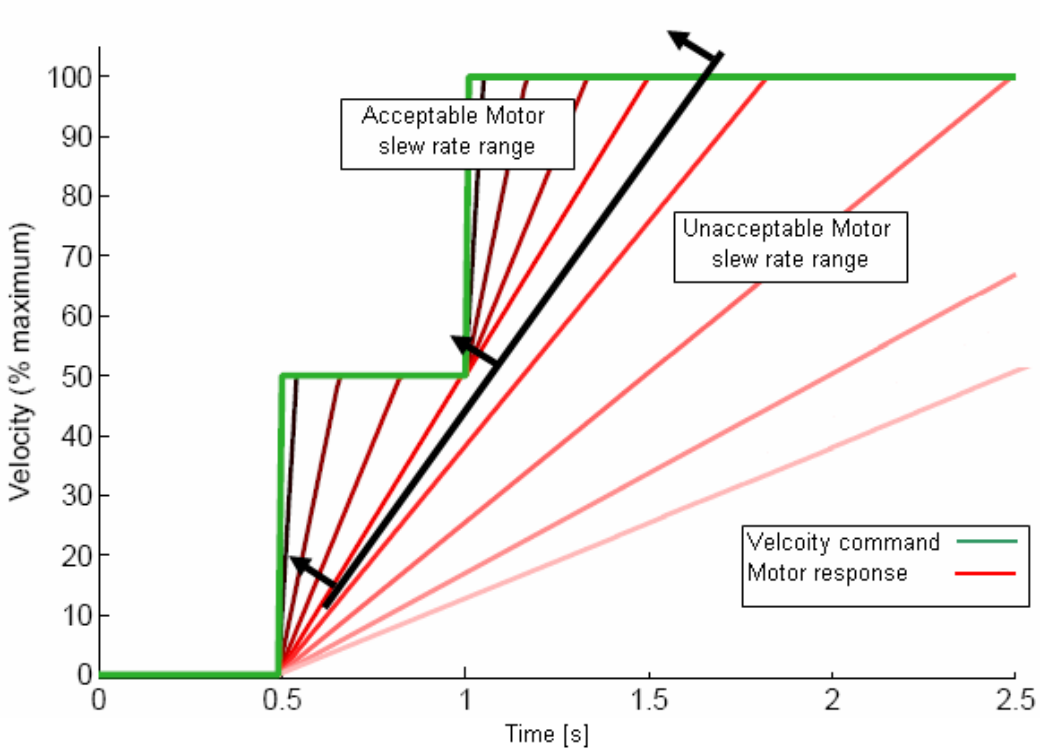

Figure 4.2 Motor slew rate effect on input shaper design [2]

Similar argument can be applied to the case when the control variable is the position of the motor rather than its speed. The linear shaper commands are superimposed to the motor response in Fig 4-3. By comparing Fig 4-2 to Fig 4-3 it is clear that the linear shaper lies in the unacceptable range, since the motor response is not fast enough to track the linear shaper command. This explains the reason the linear shaper response is identical to the unshaped response. This kind of nonlinearity was not

captured in the simple linear shaper design. However, it will be taken into account in the optimization design.

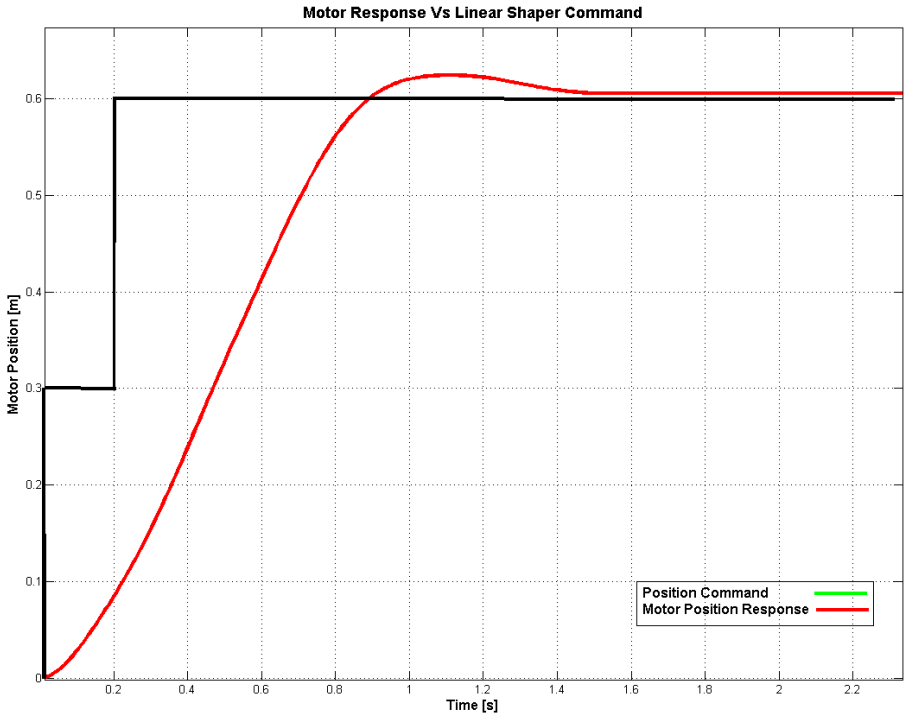

Figure 4.3 Motor Response for linear input shaper

4.2. METHODOLOGY OF INPUT SHAPER DESIGN BY OPTIMIZATION

The numerical model discussed in Chapter 2 and validated against the experimental model in Chapter 3 offers an invaluable insight of the system behavior. Using this model the time history response of the system can be evaluated for different shaper scenarios. Thanks to the computational power of today's PCs and the rapid advancements in global optimization methods, this current problem lends itself to numerical optimization. The procedure to design input shaping using optimization was addressed in the work of Meshreki [5] and proved to be fairly simple successful,

and most importantly nonlinearities can be integrated in the analysis. The basic steps are as follows:

1- Shaper is suggested by the optimization scheme (will be discussed later)
2- The numerical integration code uses the shaper parameter to return the time history response of the water level.
3- The performance of the shaper is evaluated using certain performance index according to the requirements of the problem.
4- The performance index (or objective function value in the optimization terminology) is returned to the optimization scheme to decide the next shaper parameters.

Once the optimization scheme is chosen and correctly adopted to the specifics of the problem in hand, the shaper design reduces to the identification of the requirements and formulating the performance index accordingly to reflect these requirements. The rest of this chapter will present number of input shaper design procedures. In each design, the performance index will be stated clearly and will be chosen to suit certain design criteria. The results obtained from the experimental model will be presented and discussed as well.

4.3. ZERO VIBRATION (ZV) INPUT SHAPER

Because the ZV shaper has only two variables, namely the time of the second impulse and the amplitude of the first impulse, its design is straightforward. No need to resort to complex global optimization schemes as the number of variables is very limited. In the case of ZV, Optimization can be performed by enumeration of all possible combinations in the feasible range and selecting the best results by searching

for the minimum value of the performance index. Thus the problem reduces to finding the feasible range of each of the two variables, and choosing the performance index.

In the present study the range for the time of the second impulse is taken from 0.2 to the settling time of the motor in the unshaped case. In section 4.1 it was shown that a second impulse at 0.2 does not affect the performance of the system. The enumeration step is taken to be equal to the digital resolution of the experimental controller (0.01s). As for the first impulse amplitude, a plausible range would be from 0 to 1. However, it is unlikely that the first impulse would be outside the range of 0.25 to 0.75. The enumeration step is 0.015. This step corresponds to 1 mm in the case of 0.6 m final value. Thus, for the aforementioned ranges of the two variables, the search space becomes 3570 possible scenarios. Given that the single run of the objective function takes around 0.3 s, the total run time is expected to be in the order of 18 to 20 minutes on an average PC. This is an acceptable optimization computational time, especially that enumeration will give the exact solution not a near optimum solution as in the case of global optimization schemes. It is worth noting that the choice of the upper and lower limits of the feasible range, and the search step, for the enumeration might changes according to the constraints and limitations of each design problem. The discussion above is only to provide an example of the rational behind choosing the values of the limits and search steps. Different ranges might be used for other situations. For example, had the computational time been prohibitively long, tighter ranges could have been used according to the requirements of the problem. The performance index was chosen to be simply the maximum amplitude of the residual vibration after the settling time of the motor.

The maximum amplitude of the residual vibration is more is affected by the second impulse timing (T_2) more than it is affected by the amplitude of first impulse (A_1). This is predicted since the input shaping is generally more sensitive to parameters dependent on the natural frequency of the system (T_2 in this case) than it is sensitive to parameters dependent on the damping ratio (A_1 in this case, as shown in equation 1-10). This is evident from Fig 4-4 which shows a 3D plot of the residual vibration amplitude Vs T_2 and A_1. The slope in the A_1direction is relatively small, and smooth, while, the function is harmonic in the T_2 direction.

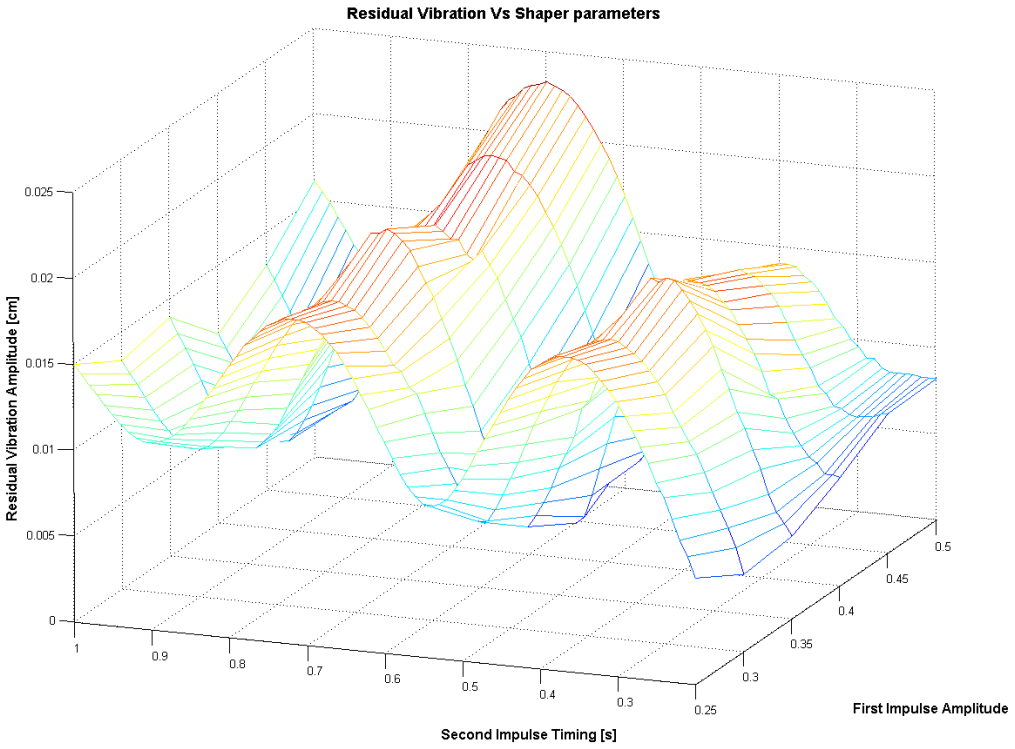

Figure 4.4 Residual Amplitude of slosh Vs. ZV Input shaper parameter

To illustrate the effect of T_2 more, the maximum residual amplitude is plot Vs T_2 while A_1 is held constant at its value that corresponds to the global minimum. The plot is shown in Fig 4-5

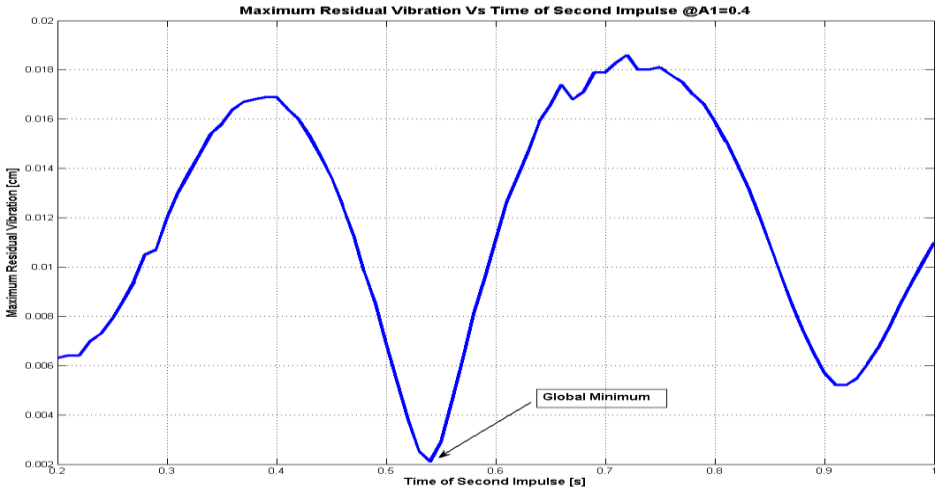

Figure 4.5 ZV shaper global optimum using enumeration

4.3.1. ZV PERFORMANCE IN THE TIME DOMAIN

The experimental results for the zero vibration shaper designed based on the enumeration optimization is shown in Fig 4-6. The parameters of the ZV shaper are listed in Appendix C.

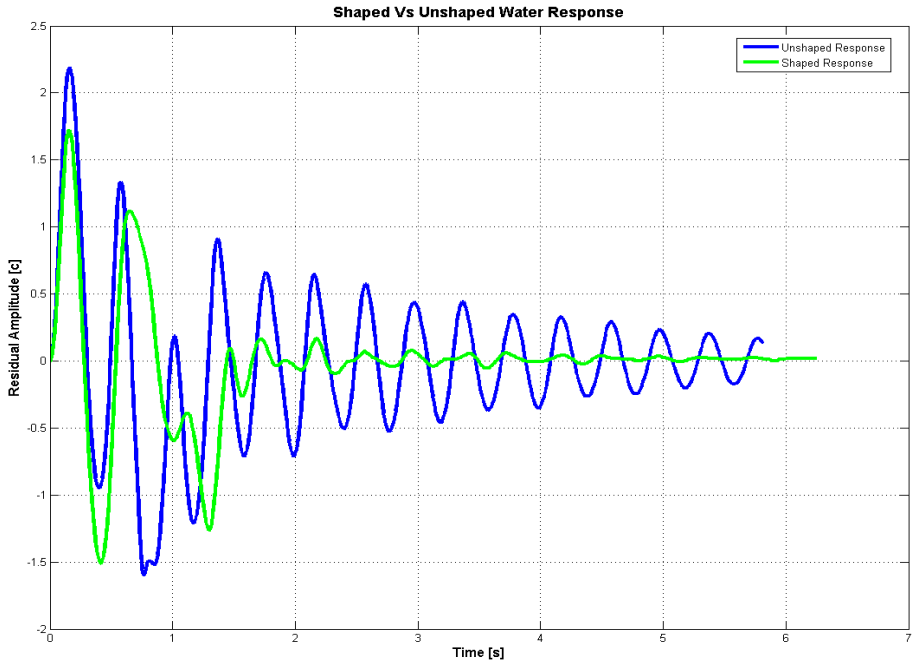

Figure 4.6 ZV Shaper Vs Unshaped water response

The maximum residual vibration amplitude after the motor settling time in the unshaped case was 0.92 cm. This value was reduced to 0.16 cm after applying the input shaper. Thus, the shaper succeeded in eliminating 82% of the residual amplitude. The reduction of the residual vibrations comes at the cost of increasing the motor settling time as shown in Fig 4-7 from 1.01 sec in the unshaped case to 1.34 sec in the shaped case.

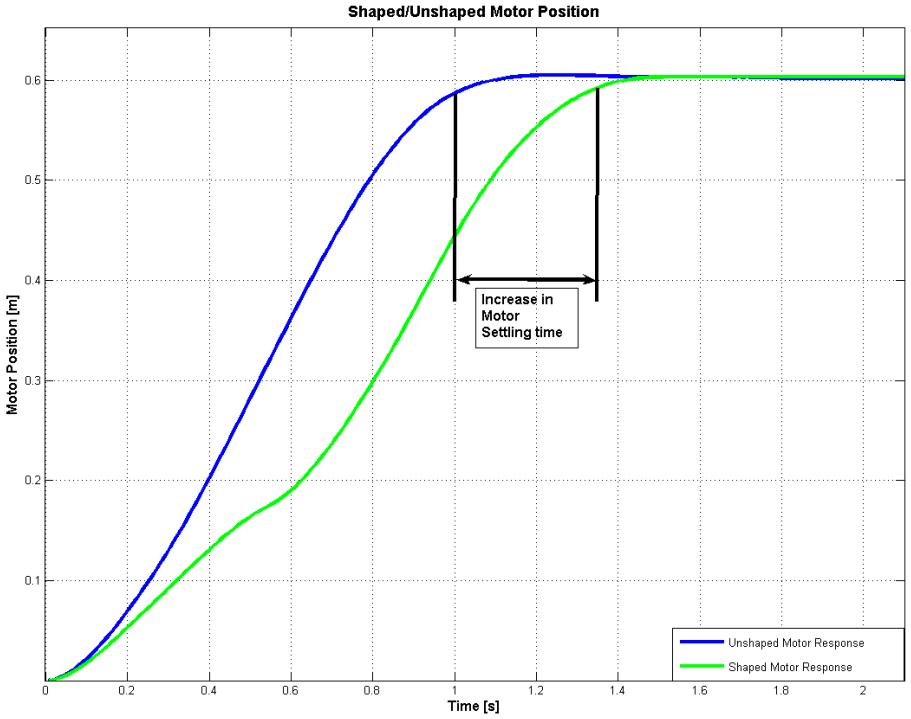

Figure 4.7 ZV shaper increase in motor settling time

4.3.2. ZV Performance in The Frequency Domain

Similar to Chapter 3, more insight can be gained by examining the response spectrum of the residual vibration. Fig 4-8 shows the frequency spectrum of the residual vibration of the shaped command together with the unshaped command.

The experimental frequency spectrum shown in Fig 4-8 conforms perfectly to the theory. The action of the input shaper is even more evident in the frequency domain

than it is in the time domain, since input shaping is essentially a filtering technique. The first mode is more accentuated in the unshaped plot than it was in Fig 3-7, since the FFT analysis is performed for the residual vibration after the settling of the motor only, and not the entire response. Therefore, the water vibration signal is not corrupted by the tank movement.

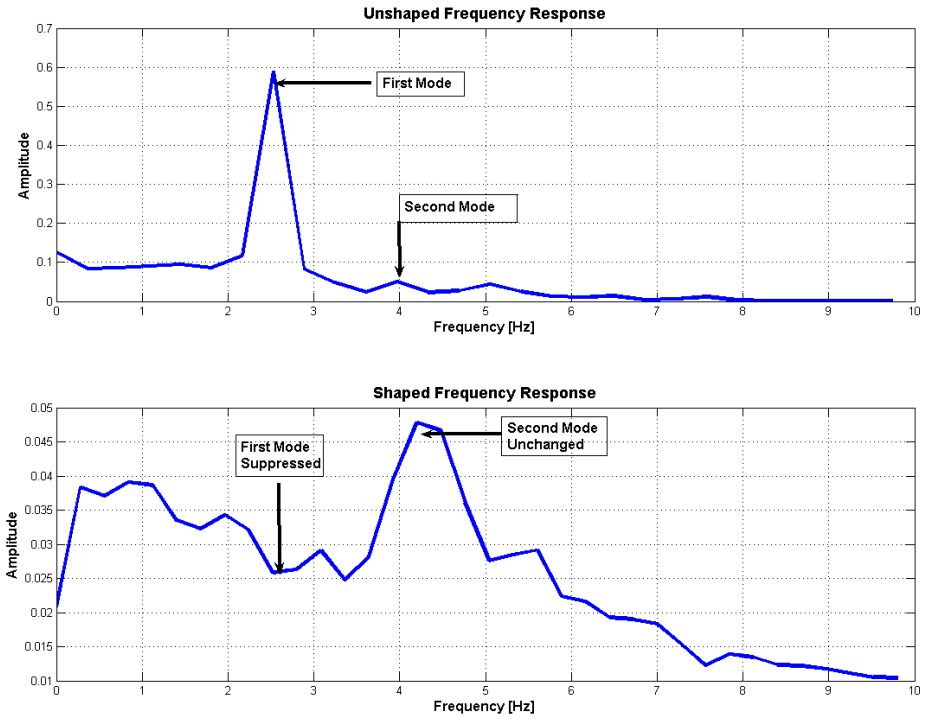

Figure 4.8 Frequency spectrum of the experimental residual vibration for the shaped and Unshaped runs

The second and third modes of vibration appear also very close to their theoretical value. On the other hand, the first mode of vibration in the shaped spectrum response was largely suppressed. The amplitude of the vibration corresponding to the first natural frequency was reduced from a magnitude 0.6 in the unshaped spectrum response, to a magnitude of 0.047 in the shaped spectrum response. This is a reduction of 91%. From the previous subsection the time domain analysis showed a reduction in the residual vibration of 82%. The difference between the two values is due to the fact that the first mode accounts for 88% of the magnitude of the residual

vibration in the unshaped case. Thus, the observed 82% reduction of the absolute magnitude of the residual vibration in the time domain is the expected value based on the frequency spectrum response. The second mode of vibration remained unchanged after the application of the shaper. This is very clear in Fig 4-8 where it is shown that the second mode value changed only from 0.05 in the unshaped response, to 0.045 in the shaped response.

The fact that the input shaper succeeded to eliminate the first mode only and not the second mode is expected, since the ZV shaper has only one degree of freedom. The filtering in ZV shaper is done by two impulses only. Therefore, only one signal can be suppressed at a time. Since the first mode is the dominant wave in the unshaped residual vibration the optimization gave the shaper that would suppress the first mode only.

Multi-mode shapers are mentioned repeatedly in literature [3] and can be designed easily by increasing the degree of freedom of the shaper. This is done by designing a shaper for each mode and convolving the two shapers together to give a four impulses shaper that is capable of suppressing the first and second modes. However, for most practical applications in sloshing, the first (or fundamental) mode is dominant and is sufficient to reduce the residual vibration of the liquid.

4.3.3. ZV SENSITIVITY

The main advantage of ZV input shaper is the simplicity and straightforwardness of the design procedure. However, this simplicity comes at the cost of increased sensitivity to modeling errors or parameters variation as discussed earlier. In Chapter 1 it was shown in Fig. 1-6 that for a typical second order system, input shaper performance degrades sharply for a change or measurement error of the natural

frequency of a mere $\pm 3\%$. Therefore, to examine the applicability of the input shaper presented in this section, sensitivity has to be studied and accounted for in the shaper design.

In the literature review in Chapter 1, it was shown in [1] that linear ZV shapers are more sensitive to errors in the natural frequency than they are to errors in the damping ratio. In the Cart/Tank model at hand, the height of the water is the variable that controls the natural frequency of sloshing of the liquid inside the tank. Fig 4-9 shows the variation of the natural frequency versus the water height in the tank.

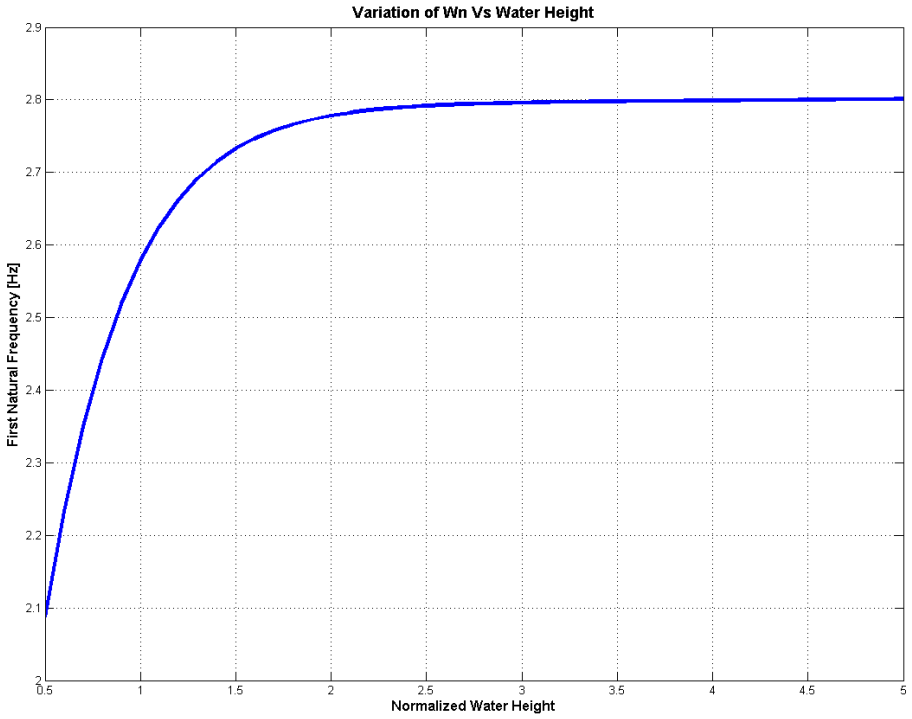

Figure 4.9 Effect of water height on the fundamental natural frequency of the water inside the tank

Fig. 4-9 is constructed for a tank with the same dimensions as the experimental setup, and water height ranges from 50% up to 500% of 4 cm. It is clearly evident that natural frequency saturates at a value of 2.8 as the normalized water height increases,

while decreases sharply for values of the height less than 4 cm. The graph shown in Fig 4-9 is the key to interpret the results shown in Fig. 4-10.

Figure 4-10 is the result of numerical simulation. The optimum shaper designed in this section is applied to the Tank/Cart model while varying the water height in the tank from 50% of the design height (4 cm) up to 300% of the design height. The maximum amplitude of the residual vibration is recorded and drawn on the y axis. The minimum value is at a normalized height of 1 as expected. The curve saturates for values greater than 1 while shoots up for values less than 1. This conforms to the results obtained from the frequency plot in Fig. 4-9.

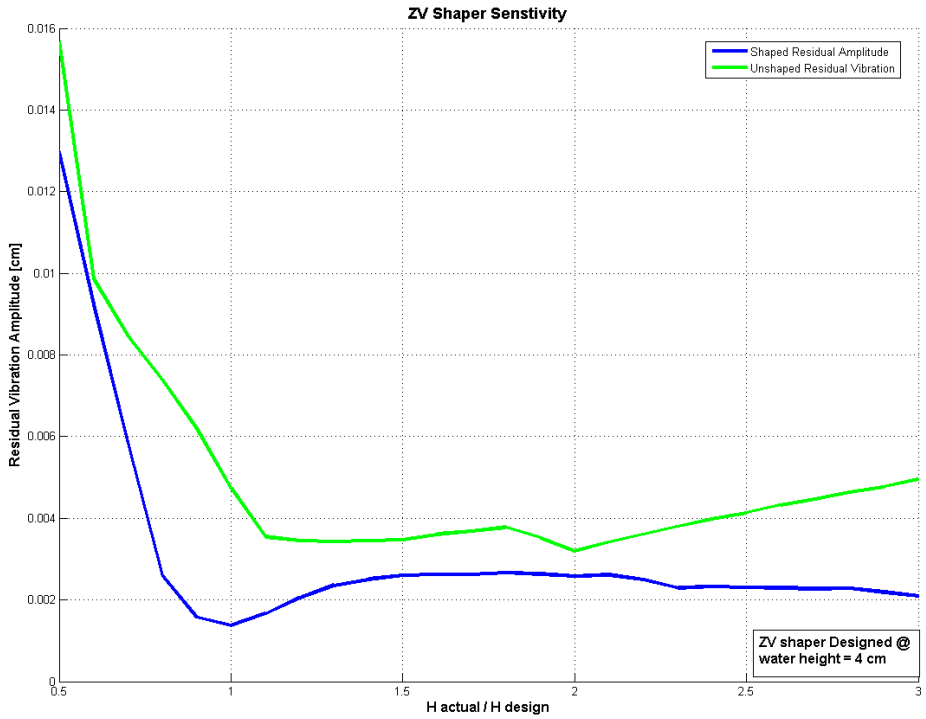

Figure 4.10 Numerical Simulation of ZV/Unshaped Maximum Residual Amplitude of vibration at different operating water heights

The maximum residual amplitude shown in Fig. 4-10 is for the absolute values of the residual vibration recorded in cm. Fig. 4-11 shows the residual amplitude in a relative manner as a percentage of the unshaped command's residual amplitude.

At the design height the percentage residual vibration of the shaped command is around 28% of the unshaped command. However, this percentage increases sharply for changes of the water height in both directions. Shaper results in detrimental effects for heights less than 50% of the design height, since the percentage exceeds 100%.

Fig. 4-10 and Fig. 4-11 together give insight into the ZV shaper performance at water heights different from the height the shaper is designed at. Fig. 4-10 suggests that for water heights less than the design height, the residual water sloshing will increase in magnitude, while for heights larger than the design height the magnitude of the residual sloshing will largely saturate.

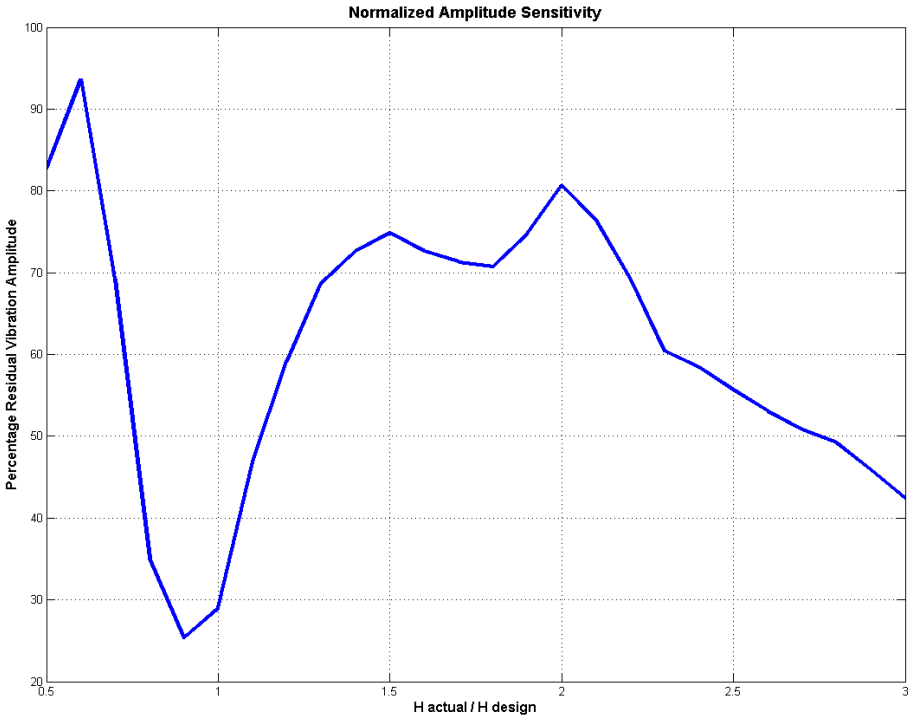

Figure 4.11 Numerical Simulation of ZV percentage reduction of residual vibration compared to the unshaped case at different operating heights

On the other hand, Fig.4-11 suggests that the effectiveness of the ZV input shaper, characterized by the ability of the shaper to reduce the residual amplitude compared to an unshaped command, will deteriorate for changes in the water height both in the positive as well as the negative directions.

In practical applications the emphasis is placed on the absolute value of residual vibration. It is usually the interest of the designer to maintain the residual amplitude at its minimum regardless of the effectiveness of the shaper. Also, in most practical applications of moving tanks filled with liquid in production lines, liquid is poured out of the tank and the its height is reduced over the production cycle. Therefore the need arises for designing input shapers that are insensitive for water height changes especially in the negative direction.

4.4. ZERO VIBRATION DERIVATIVE (ZVD) INPUT SHAPER

As mentioned in Chapter 1, the problem of shaper sensitivity has been tackled in the literature by adding an extra constraint in the design of the shaper in addition to the traditional zero vibration constraint. The additional constraint is to set the derivative of the residual vibration with respect to a certain model parameter, typically the natural frequency, to zero. This has the effect of flattening the sensitivity curve near the modeling parameter, which improves the insensitivity of the shaper to changes in this parameter as shown in Fig. 1-6. The cost of adding extra constraint is that an extra degree of freedom has to be added as well. Therefore, the length of shaper is increased from 2 impulses in the case of ZV to 3 impulses in the case of ZVD. A 3 impulses shaper has 6 variables. However, since first amplitude timing is taken at zero and the 3 amplitudes are constrained to sum up to unity, the number of variables of the ZVD reduces to 4.

The four variables of the ZVD preclude the use of enumeration to determine the optimum shaper. Therefore, more elaborate optimization scheme has to be employed. Given the harmonics shown in Fig. 4-4 of the residual vibration amplitude case of the two dimensional ZV. It is obvious that local search methods will get trapped in one of

the local minima and miss the global minimum. Because of the limited number of variables, and the expected harmonic nature of the objective function, it was decided to use real-coded genetic algorithms (GA) [24].

There are mainly two challenges in optimization problems. First, to transform the qualitative design requirements into a quantitative performance index, in order to be able to state an objective function that captures all the elements of the design requirements. Second, the optimization scheme itself has to be fine-tuned based on the characteristics of the problem at hand. Appendix B lists the various parameters employed in the present GA scheme, together with a sample plot showing GA convergence.

4.4.1. ZVD OBJECTIVE FUNCTION

As mentioned above the first step to build an objective function is specifying the design requirements in a qualitative manner. For the case of the ZVD, the design requirements are:

1-Creating minimum residual vibration at the design water height.

2-Should the water height decrease, the ZVD has to remain effective in suppressing the residual vibration.

3-The shaper time should be minimal to avoid the trivial solution of achieving good residual amplitude response at the cost of increasing the motor settling time indefinitely.

Having stated the design requirements, they can now be transferred into mathematical relations that describe the performance of each shaper. Later, the terms representing each requirement will be manipulated and normalized to suit the optimization scheme.

The first requirement is represented by the largest magnitude of the residual vibration after the settling of the motor. Other variables have been tried such as the water settling time, and average magnitude of residual oscillations. However, the largest magnitude was found to represent this design criterion more accurately. Equation 4-1 shows this condition,

$$obj1 = \max(U_{t=T_s}^{t=T_f}) \qquad \text{At } H_{operating} = H_{design} \qquad \text{4-1}$$

where U is the time response of the displacement of the extreme node of the FE numerical model, T_s is the settling time of the motor, T_f is the final time value. The response U is taken for water level height in the tank equals to the design water level height.

The second design requirement stated at the beginning of this subsection has to do with the robustness of the ZVD shaper. The shaper has to be able to suppress the sloshing residual vibrations at water heights that are less than the design height. Fig. 4-10 shows the water maximum amplitude of residual vibration on the Y axis as a function of the water height in the tank normalized by the height the shaper is designed for, 4 cm in this case, on the X axis. It is evident that the function is decreasing almost linearly at the region between 0.5 and 1 on the X axis. The objective of the ZVD is to flatten this slope.

Numerous objective functions representing this criterion have been suggested and tried. These functions will be briefly mentioned here for completeness. However, the

results will be shown only for the function that was thought to be giving the best results for the scope of this study.

One suggestion for this part of the objective function was the backward numerical derivative of the residual amplitude of vibration with respect to water height in the tank. This is a straightforward line of thinking, since it is a replication of the linear zero vibration derivative constraint expressed in numerical format. However, this objective function was not suitable for the optimization scheme. This is mostly attributed to the non-uniform behavior of the ZVD shaper in the specified design range, namely the 0.5 → 1 of the normalized water height on the X axis. While Fig 4-10 shows almost a straight line with constant negative slope for the sensitivity of the ZV shaper in the design range, the ZVD shaper's sensitivity response is not uniformly linear. In fact as will be shown later in this Chapter, for the optimum ZVD, the sensitivity curve slope changes direction in this range Fig. 4-12. Such non-uniform behavior can not be captured by the simple backward numerical differentiation.

Another objective function suggested was similar to the specified insensitivity (SI) input shaper proposed by Singhose in [8]. In this function, a tolerable level of the increase of the residual sloshing amplitude as a percentage of the minimum amplitude at the design height is specified by the designer. For example the designer states that values greater than 25% increase in the residual vibration amplitude due to changes in the water height are unacceptable. In this case the objective function solves for the height that satisfy this requirement. The height is incorporated in the objective function so that the optimization scheme maximizes it. The advantage of this objective function is that it turns the insensitivity into a design variable. However, the function was numerically exhaustive. Also, the part where the function solves for the

height that satisfies the specified level of insensitivity suffered from numerical problems, due to the multiple zero crossings of the function.

Finally it was decided to express the robustness part of the objective function in a simple format, which proved successful at the end. Similar to the first design requirement, the robustness part of the objective function was stated as the residual amplitude shaped command at 75% and 50% of the design height. This is shown in equation 4-2

Obj2 = (Residual Amplitude @ 0.5 H_{design}) + (Residual Amplitude @ 0.75 H_{design})

4-2

The last part of the objective function mentioned at the beginning of this subsection has to do with the settling time of the motor. This is a straightforward part of the objective function. It was represented by the increase of the settling time of the motor in the shaped command compared to the unshaped command. This is shown in equation 4-3

$$Obj3 = (T_{s\,(shaped)} - T_{s\,(unshaped)}) \qquad 4\text{-}3$$

Equations 4-1 through 4-3 are the three parts of the objective function. However, in order to be able to add them algebraically, all three objectives must have comparable magnitudes, so that no one objective dominates the others. This was done by normalizing the three objectives as will be shown. Factors were added to give different weight for each objective according to the requirements of the problem. The final version of the objective function is stated hereunder.

$$obj = \sum_{i=1}^{3} k_i \times \frac{\max(U_{t=T_s}^{t=T_f})_{shaped} @ h = c_i \times h_{nominal}}{\max(U_{t=T_s}^{t=T_f})_{unshaped} @ h = c_i \times h_{nominal}} + k_4 \frac{\left(T_{s\,(shaped)} - T_{s\,(unshaped)}\right)}{T_{s\,(unshaped)}} \qquad 4\text{-}4$$

Where K_i is the weighting factor for each design criterion, h is the operating height, $h_{nominal}$ is the design height, C is factors vector = [1,0.75,0.5], T_s and U defined earlier in equations 4.1 and 4.3 respectively.

4.4.2. Results and Discussion of ZVD Performance

Fig. 4-12 shows numerical run of the sensitivity of the ZV and ZVD in the range from 0.5 to 3 of the design height (5 cm in this case). The actual parameters of the ZVD shaper are listed in Appendix C. The performance of the unshaped command is superimposed on the curve as well for comparison reasons. The following weighting coefficients were used in the objective function of the ZVD shaper whose curve is shown in Fig. 4-12, K_1= 3, K_2=2, K_2=2, K_3=1.

It is very clear from the figure that both the ZV and ZVD are superior to the unshaped command almost over the entire range of operation. It is also clear that the designed ZVD was successful in reducing the residual vibration amplitude significantly in the 0.5 → 1 range. The maximum value of the ZVD residual vibration in this range was 2.75×10^{-3} m, whereas in the ZV case this value shoots to 0.01 m.

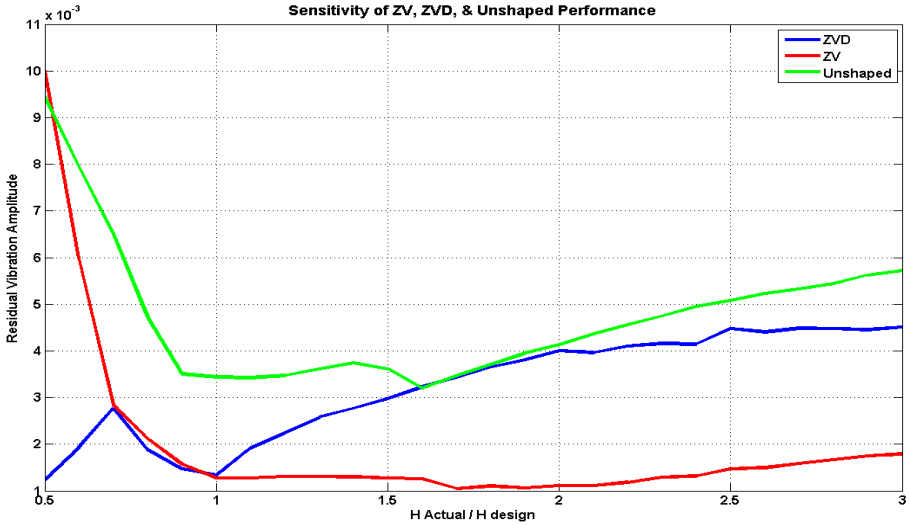

Figure 4.12 Numerical Simulation comparison of ZV/ZVD/Unshaped residual amplitude for different operating heights

This improvement in the performance comes at the cost of deteriorating performance in the range from 1 → 3, however, it still remained below the unshaped command. This deterioration is expected since no factor of the objective function reflects the performance of the ZVD shaper in that range. The improvement comes at the cost of increased motor settling time as well.

Due to limitation on the experimental setup the results showed in Fig. 4-12 could not be validated over the entire range. The maximum height of the water tank is 8 cm, given that the water sloshing during the motion of the motor is in the range of 2-3 cm the maximum operating height should not exceed 5 cm. On the other hand the minimum operating height is 3 cm. Less water height causes the sensor to hit the bottom of the tank during motion which affects the results negatively. As shown in Fig. 4-12 the residual amplitude of sloshing for both the ZV, and ZVD, is almost identical in the range from 0.7→1 on the X axis. For a design height of 5 cm this corresponds to a range of 3.5 → 5 cm. Given the physical constraints of the device, the range where the ZVD shows superior performance to the ZV is mostly unattainable.

However, in order to validate the results obtained, experiments were conducted for the ZV, ZVD designed at $H_{nominal}$ = 5 cm, and unshaped commands. The experimental data is compared to the time response of the numerical model. The results are summarized in table 4-1. The time responses (both numerical and analytical) are shown in Fig. 4.13 through Fig. 4-18.

Table 4-1 Numerical/Experimental residual amplitude for ZVD,ZV, Unshaped input

	Operating Height	Residual Amplitude (Numerical	Residual Amplitude (Experimental)
ZVD	3	0.21	0.44
	4	0.22	0.21
	5	0.15	0.1
ZV	3	0.6	0.55
	4	0.21	0.26
	5	0.13	0.21
Unshaped	3	0.79	0.66
	4	0.47	1
	5	0.34	0.5

The numerical and analytical data compares favorably, especially in relative manner. The results and plots reveal the strength of both ZV and ZVD in suppressing residual vibration, and the robustness of the ZVD shaper. It is also noticed that the ZVD results in the lowest water level throughout the entire motor motion. This property is emphasized in the next section by adding motion constraint.

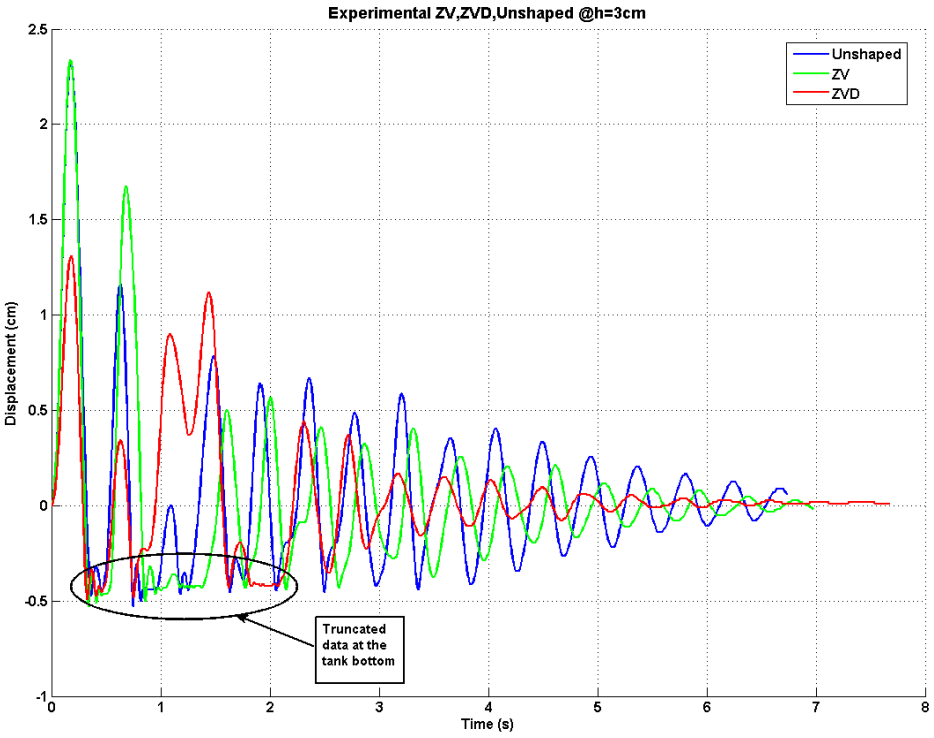

Figure 4.13 Experimental Run ZV/ZVD/Unshaped @ water height = 3 cm

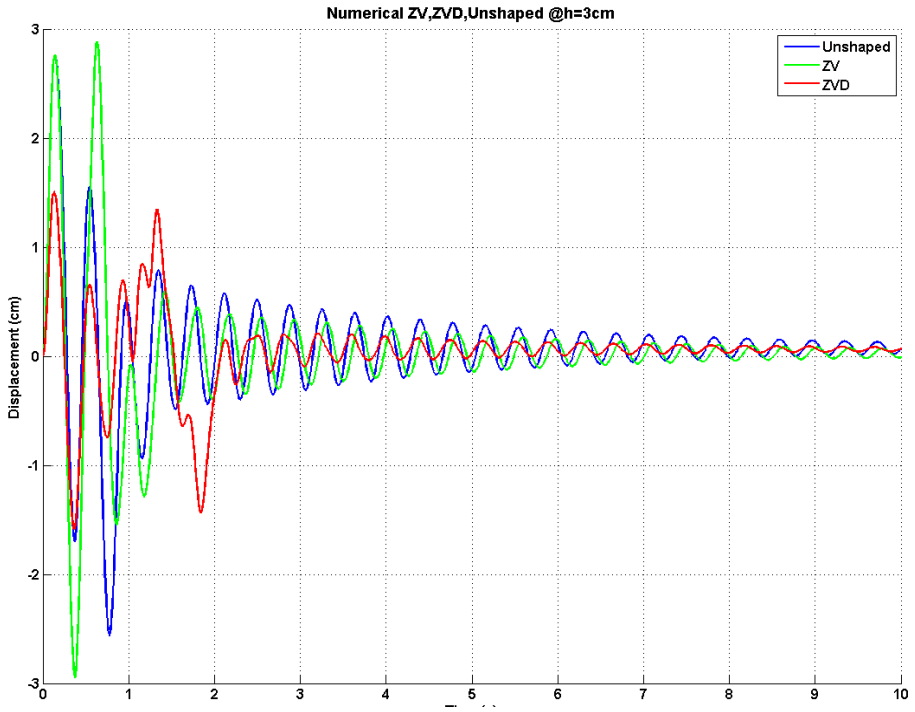

Figure 4.14 Numerical Run ZV/ZVD/Unshaped @ water height = 3 cm

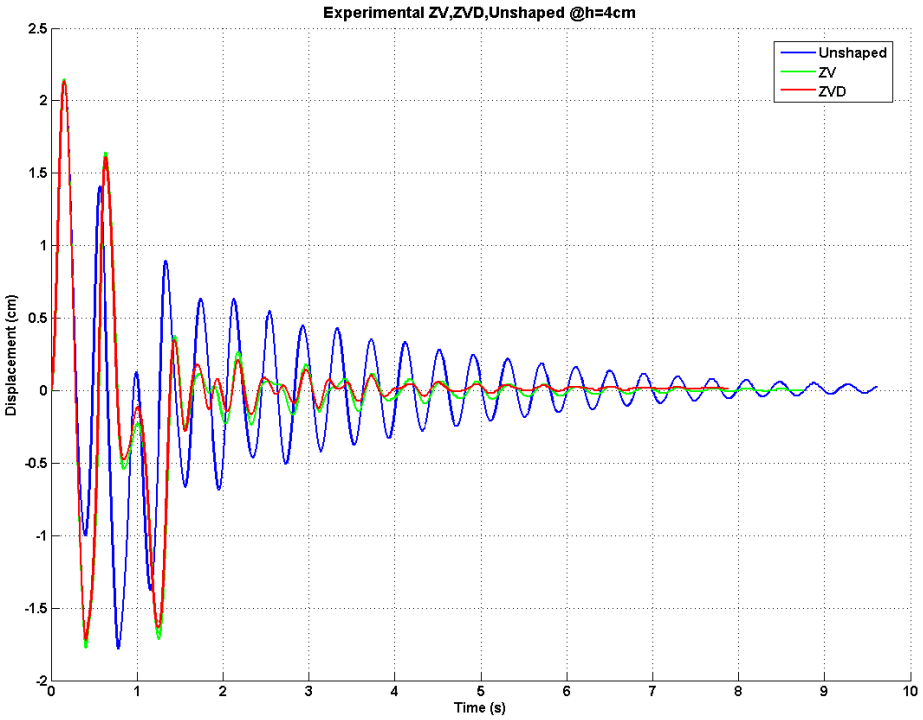

Figure 4.15 Experimental Run ZV/ZVD/Unshaped @ water height = 4 cm

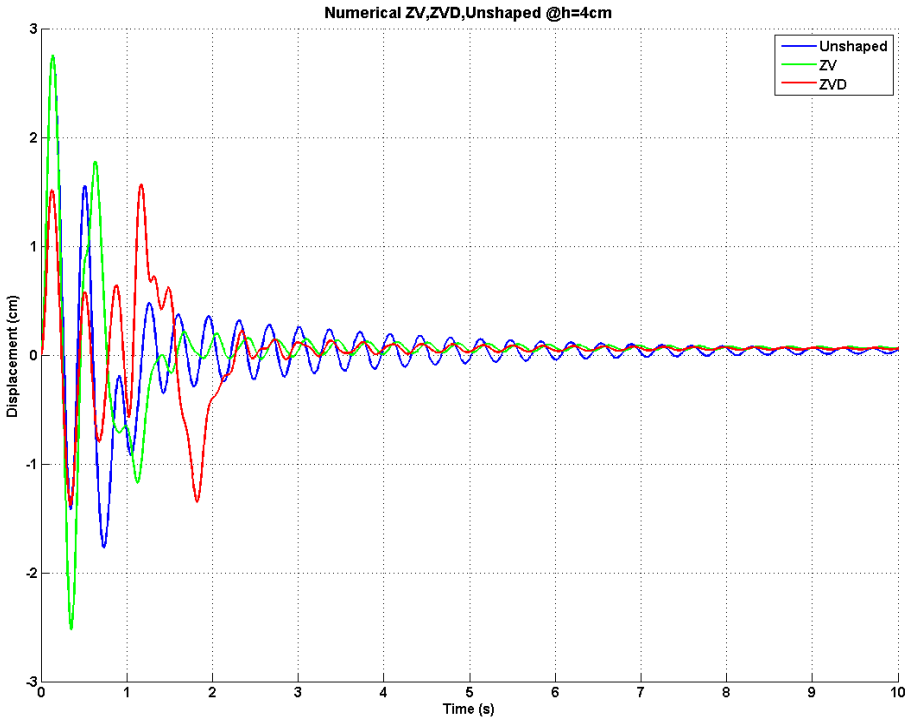

Figure 4.16 Numerical Run ZV/ZVD/Unshaped @ water height = 4 cm

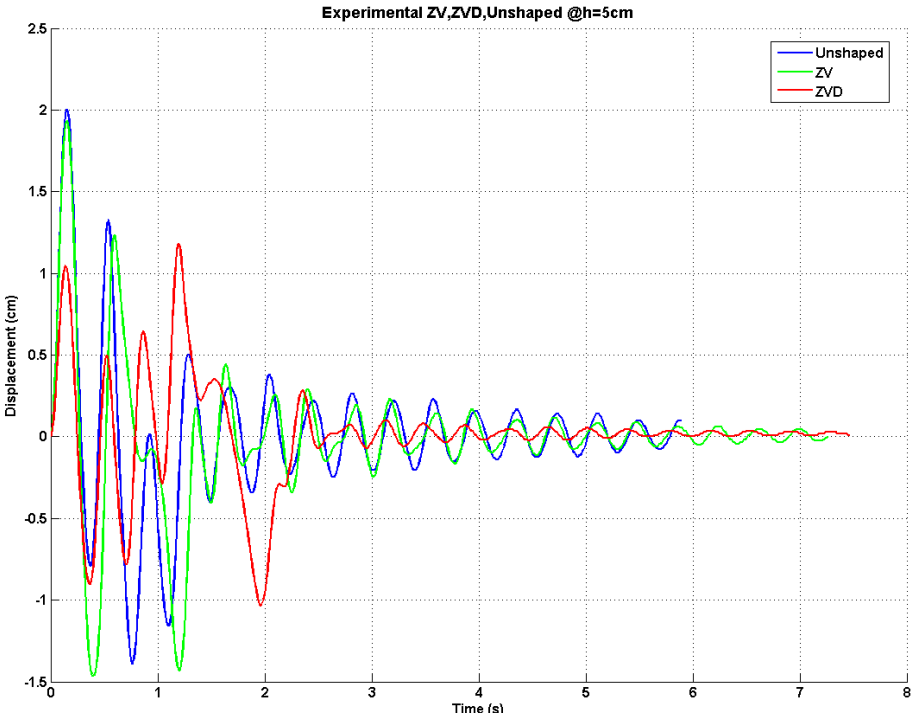

Figure 4.17 Experimental Run ZV/ZVD/Unshaped @ water height = 5 cm

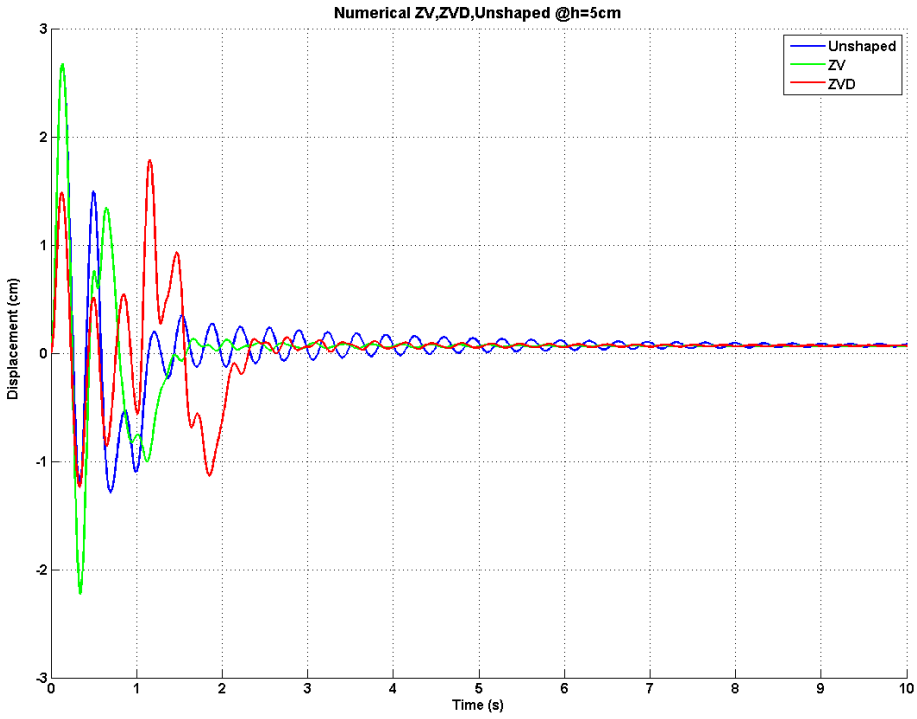

Figure 4.18 Numerical Run ZV/ZVD/Unshaped @ water height = 5 cm

Inspection of these curves reveals that both the ZV and ZVD shapers yield lower residual vibrations levels as compared to the unshaped response. Furthermore, the ZVD shaper, with its improved robustness, gives a better performance than the ZV shaper at water heights other than the one they were designed at. This also agrees well with the numerical predictions.

4.5. Deflection Limiting Input Shaper

The convenience of the numerical model, and shaper design using optimization techniques, make the addition of more objectives and motion constraints very attractive. One constraint repeatedly addressed in the literature is the deflection limiting [17]. In Deflection limiting (DL) the maximum magnitude of structural deflection is limited to a certain predefined value. This constraint is attractive in the problem of moving tank to prevent spilling.

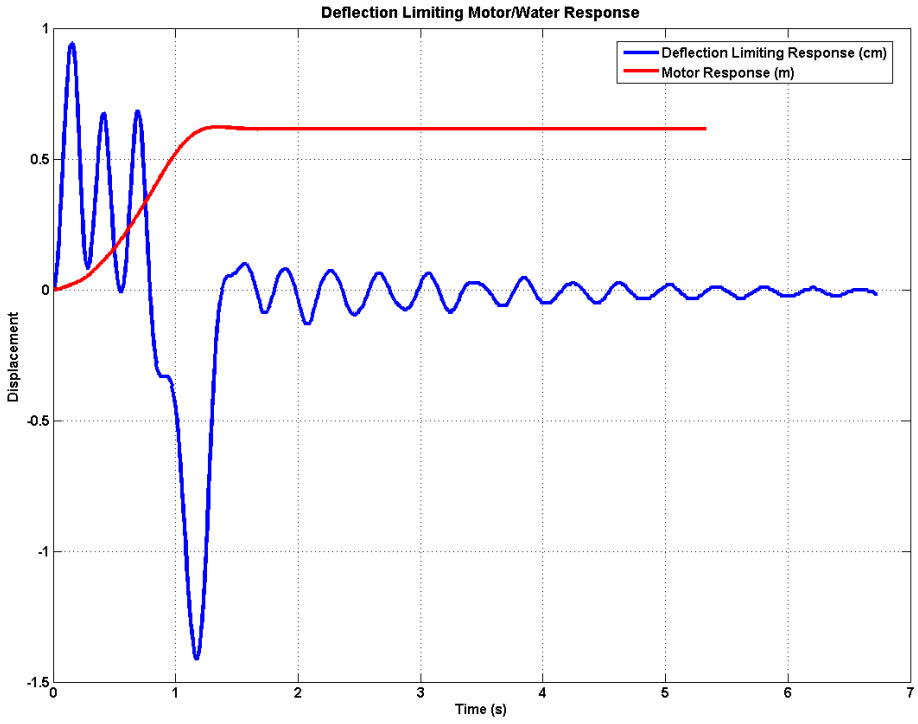

Figure 4.19 Experimental response of Deflection limiting input shaper

In the optimization scheme the DL can be expressed as a constraint, where a penalty is applied to the objective function should the maximum amplitude of vibration of any of the (FE) nodes exceeds a predefined value. Since DL is a hard constraint the weighting factors (K_i vector in equation 4.4) have to be chosen carefully to relax other objectives in favor of the constraint. For example, it is expected that the DL constraint would cause the settling time of the motor to increase. Physically, this means that fast motor maneuver and limiting the maximum sloshing of the water inside the tank are two contradicting objectives and one of them has to be relaxed to be able to accomplish the other. In the experimental run shown in Fig. 4-19 the maximum (positive) amplitude of vibration was limited to a value less than 1cm. The weighting factors applied were [3,1,1,0.5] as defined by equation 4.4. The actual parameters of the DL shaper are listed in appendix C. The graph shown in Fig. 4-19 is the experimental response of the resulting shaper. Comparing the DL response to the unshaped response in Fig 4-1 where the maximum amplitude of vibration was 2.3 cm, and the residual vibration was 0.95 cm, while these values were 0.9 cm and 0.15 cm respectively in the case of the DL shaper, shows the benefit of the input shaping technique clearly. The improved performance comes at the mere cost of 0.42 (s) increase in the motor rise time.

CHAPTER 5

CONCLUSIONS

The work presented in this thesis demonstrated how input shaping techniques can effectively be applied to mitigate sloshing effects in liquid tanks undergoing point-to-point maneuvers. To this end, the liquid behavior is modeled using finite element analysis. A numerical model was also developed to simulate the dynamics of a motor-driven cart/tank system. These models were then integrated to simulate the behavior of the coupled system. The nature of such a modeling technique permitted the incorporation of nonlinearities, such as motor saturation and friction, into the numerical model. The input shaper parameters were optimized to find the commands that would result in minimum residual vibration. The objectives were to minimize residual vibration, as well as the motor settling time. Other objectives, such as improved robustness and motion constraints, including deflection limiting, were also incorporated in the optimization scheme. An experimental setup consisting of a small motor-driven water tank that is precisely guided to undergo rectilinear motion, was built. Numerical results were shown to capture the experimental behavior quite remarkably, which validated the accuracy of the adopted methodologies. The two main input shaping techniques addressed in this work were the Zero Vibration (ZV) and Zero Vibration Derivative (ZVD) schemes. Both demonstrated improved performance over unshaped commands. While ZV was capable of reducing residual vibration by nearly 80%, its sensitivity was outperformed by the ZVD scheme, which showed a larger range of acceptable performance allowing more room for modeling errors and parameter variation. The concept of deflection limiting, originally

developed in the literature to minimize structural swaying during commanded motion was implemented herein to limit the amplitude of liquid sloshing over the entire length of the tank motion, thus reducing the chances of spilling. The results obtained suggest that input shaping is an effective method for suppressing liquid sloshing.

Suggestions for future work include tuning the objective functions, as they were found to have a considerable effect on the system performance. Other parameters in the model, such as the proportional control gain adopted in the position control loop, may be treated as optimization variable for further enhance the effectiveness. Other types of control, including PD and PID control, can also be potential candidates for improved positioning response.

REFERENCES

1-Singer, N.C. and Seering, W. P., ”Preshaping Command Inputs to Reduce System Vibration,” Journal of Dynamic Systems, Measurement and Control, Proceedings of the American Society of Mechanical Engineers, Vol. 112, pp.76-82, 1990.

2-Sornesen, K. L., A Combined Feedback and Command Shaping Controller for Imporving Positioning and Reducing Cable Sway in Cranes, Masters Thesis, Georgia Institute of Technology, USA, 2005

3-Singhose, W. E., *Command Generation for Flexible Systems*, Ph.D. Thesis, Massachusetts Institute of Technology, 1997.

4-Terashima, K. and Yano, K., “Sloshing Analysis and Suppression Control of Tilting-type Automatic Pouring Machine,” *Control Engineering Practice*, Vol. 9, pp. 607-620, 2001.

5-Meshreki, M. A. H., *Design Methodology for Input Shapers Using Genetic Algorithms in Flexible Nonlinear Systems*, Masters Thesis, American University in Cairo, Egypt, 2004.

6-Smith, O. J .M., “Posicast Control of Damped Oscillatory Systems,” *Proceedings of the IRE*, pp. 1249-1255, 1957.

7-Singhose, W., Derezinski, S. and Singer, N., “Extra-Insensitive Input Shapers for Controlling Flexible Spacecraft,” *J. of Guidance, Control, and Dynamics*, 2, 1996, pp. 385-91.

8-Singhose, W.E., Seering, W.P. and Singer, N.C., “Input Shaping for Vibration Reduction with Specified Insensitivity to Modeling Errors,” *Japan-USA Sym. on Flexible Automation*. Boston, MA, 1996.

9-Cutforth, C. F. and Pao, L.Y., "Adaptive Input Shaping for Maneuvering Flexible Structures," *Automatica*, Vol. 40, pp. 685-693, 2004.

10-Bodson, M.,"An Adaptive Algorithm for the Tuning of Two Input Shaping Methods," *Automatica*, Vol. 34, No. 6, pp. 771-776, 1998.

11-Kojima, H. and Singhose, W., "Adaptive Deflection-Limiting Control for Slewing Flexible Space Structures," *Journal of Guidance, Control and Dynamics*, Vol. 30, No.1, 2007.

12-Sorensen, K. and Singhose, W., "Oscillatory Effects of Common Hard Nonlinearities on Systems Using Two-Impulse ZV Input Shaping," *Proceedings of the 2007 American Control Conference*.

13-Lawrence, J., Hekman, K. and Singhose, W., "An Analytical Solution for a Zero Vibration Input Shaper for Systems with Coulomb Friction," *Proceedings of the 2002 American Control Conference*, Vol. 5, pp. 4068-4073, 2002.

14-Mohamed, Z. and Tokhi, M.O., "Hybrid Control Schemes for Input Tracking and Vibration Suppression of a Flexible Manipulator," *Proceedings of the Institution of Mechanical Engineers*, Vol. 217, Part I, Journal of Systems and Control Engineering, pp. 23-34, 2003.

15-Sorensen, K., Singhose, W. and Dickerson, S., "A Controller Enabling Precise Positioning and Sway Reduction in Bridge and Gantry Cranes" *Control Engineering Practice*, Vol. 15, pp. 825-837, 2007.

16-Banerjee, A.K., "Dynamics and Control of the WISP Shuttle-Antennae System," *J. of Astronautical Sciences*, 1, 1993, pp. 73-90.

17-Singhose, W., Banerjee, A. and Seering, W., "Slewing Flexible Spacecraft with Deflection-Limiting Input Shaping," *J. of Guidance, Control, and Dynamics*, 2, 1997, pp. 291-298.

18-Park, S., Kim, B. K. and Youm, Y., "Single-Mode Vibration Suppression for a Beam-Mass-Cart System Using Input Preshaping with a Robust Internal-Loop Compensator," *Journal of Sound and Vibration*, Vol. 214, No. 4, pp. 693-716, 2001.

19-Feddema, J., Dohrmann, C. and Parker, G., Robinett, R., Romero, V. and Schmitt, D., "A Comparison of Maneuver Optimization and Input Shaping Filters for Robotically Controlled Slosh-Free Motion of an Open Container of Liquid," *Proceedings of the 1997 American Control Conference*, Vol. 3, pp. 1345-1349, 1997.

20-Arafa, M., "Finite Element Analysis of Sloshing in Rectangular Liquid-filled Tanks," *Journal of Vibration and Control*, Vol. 13, No. 7, pp. 883-903, 2007.

21-www.qunser.com/english/downloads/toolbx/labs/May,2002/Linear%20%20Self%20Erecting%20Inverted%20Pendulum%20(IP02).pdf

22-Abramson, H.N., 1966, *The Dynamic Behavior of Liquids in Moving Containers*, NASA SP-106, Washington, D.C., updated by F.T. Dodge, Southwest Research Institute, 2000.

23-Ibrahim, R.A., Liquid Sloshing Dynamics: Theory and Applications, Cambridge University Press, 2005.

24-Herrera, F., Lozano, M. and Verdegay, "Tackling Real-Coded Genetic Algorithms: Operators and Tools for Behavioral Analysis" *Artificial Intelligence Review*, Vol. 12, pp. 265-319, 1998.

APPENDICES

APPENDIX A: EXPERIMENTAL PARAMETERS

Table A-1: Experimental setup parameters, tuning factor and sensors resolution

Cart Mass (Kg)	M_{cart}	0.815
Motor Armature Resistance (ohm)	Rm	2.6
Back emf constant (volt/rad s^{-1})	Km	0.00767
Gear box ratio	Kg	3.7
Motor pinion gear (m)	r	0.00635
Back emf tuning factor	C_2	1.1
Volt tuning factor	C_1	0.9
Cart velocity threshold value (m/s)		0.025
Cart friction coefficient	μ	0.01
Motor saturation voltage (volt)		±5
Cart encoder resolution (count/rev)	-	512 * 4
Cart encoder calibration const. (cm/count)	-	0.00454
Water level encoder resolution (count/rev)	-	1024*4
Water level encoder calibration const. (cm/count)	-	0.0087

APPENDIX B: GA PARAMETERS

Table B-1: GA basic parameters used in optimization

Number of variables	4
Population size	60
Number of generation	20
Uniform mutation	4
Boundary mutation	4
Arithmetic cross over	2
Simple arithmetic	2
Whole non-uniform mutation	4
Heuristic cross over	2
None uniform mutation parameter	6
Simple cross over parameter	10
Q	0.1

APPENDIX C: OPTIMUM SHAPERS PARAMETERS

Table C-1: Optimum parameters for ZV,ZVD,DL shapers

	Design h (cm)	A_1	A_2	t_2	t_3
ZV	**4**	0.4	-	0.52	-
Linear ZV	**4**	0.5	-	0.19	-
ZVD	**5**	0.2	0.19	1.02	1.22
DL	**4**	0.167	0.22	0.22	0.44